

Fundamental Properties of Novae in M31

ALLEN W. SHAFTER  ¹ AND KAMIL HORNOCH  ²

¹Department of Astronomy and Mount Laguna Observatory, San Diego State University, San Diego, CA 92182, USA

²Astronomical Institute of the Czech Academy of Sciences, Fričova 298, CZ-251 65 Ondřejov, Czech Republic

ABSTRACT

The peak luminosities and rates of decline for a large sample of novae recently published by Clark et al. have been analyzed using the Yaron et al. nova models to estimate fundamental properties of the M31 nova population. The apparent white dwarf (WD) mass distribution is approximately Gaussian with a mean $\langle M_{\text{WD}} \rangle = 1.16 \pm 0.14 M_{\odot}$. When corrected for recurrence-time bias, the mean drops to $\langle M_{\text{WD}} \rangle = 1.07 M_{\odot}$. The average WD mass of the M31 nova sample is found to be remarkably similar to that found by Shara et al. in their study of 82 Galactic novae, but $\sim 0.15 M_{\odot}$ more massive than the mean recently determined by Schaefer in his comprehensive study of more than 300 systems. As expected, the average WD mass for the recurrent novae included in the M31 sample, $\langle M_{\text{WD}} \rangle = 1.33 \pm 0.08 M_{\odot}$, is significantly higher than that for novae generally. Other parameters of interest, such as the accretion rate, velocity of the ejecta, and the predicted recurrence time, are characterized by skewed distributions with large spreads about means of $\langle \log \dot{M} (M_{\odot} \text{ yr}^{-1}) \rangle \simeq -9.27$, $\langle V_{\text{max}} \rangle \simeq 1690 \text{ km s}^{-1}$, and $\langle \log P_{\text{rec}} (\text{yr}) \rangle \simeq 4.39$, respectively. The role of hibernation in affecting the \dot{M} and P_{rec} distributions is briefly discussed. Finally, the nova properties were studied as a function of apparent position (isophotal radius) in M31, with the preponderance of evidence failing to establish any clear dependence on stellar population.

Keywords: Andromeda Galaxy (39) – Cataclysmic Variable Stars (203) – Novae (1127) – Recurrent Novae (1366) – Time Domain Astronomy (2109)

1. INTRODUCTION

Nova eruptions result from a thermonuclear runaway (TNR) on the surface of an accreting white dwarf (WD) in a close binary system. The mass donor, commonly referred to as the secondary star because it is the less massive component, fills its Roche lobe and transfers material to the WD (the primary) via an accretion disk. As the material accumulates on the WD, the temperature and density at the base of the accreted layer increase to the point where hydrogen burning can commence. If the material is deposited sufficiently slowly ($\lesssim 10^{-6} M_{\odot} \text{ yr}^{-1}$), it will become at least partially degenerate prior to Hydrogen ignition, resulting in a TNR (e.g., see Shara 1989; Starrfield et al. 2016, and references therein). The explosion and subsequent ejection of all or part of the accreted material leads to an eruption that can reach an absolute magnitude of $M_V \sim -10$, making novae among the most luminous transient sources known.

After a nova event, accretion onto the WD eventually resumes and the process repeats over timescales that can be as short as a year (e.g., see Darnley et al. 2014; Tang et al. 2014). Ford (1978) has shown that a significant fraction of nova progenitors must undergo multiple outbursts in order to explain the observed nova rate in M31. Systems with relatively short intervals between successive eruptions, $P_{\text{rec}} \lesssim 100 \text{ yr}$, and where more than one eruption has been observed, are referred to explicitly as “Recurrent Novae” (RNe).

The observed properties of novae, such as their peak luminosities and subsequent rates of decline (typically parameterized by t_2 , the time in days to decline by 2 mag from maximum light), the maximum velocity of the ejected material

and the recurrence time depend critically on at least two parameters of the progenitor binary: the mass of the WD, and the rate of accretion onto its surface, with the latter being important for determining the temperature of the accreted layer. Theory and models have shown that massive WDs accreting high rates only need to accrete a relatively small amount of material (the ignition mass, $M_{\text{ign}} \lesssim 10^{-5} M_{\odot}$) before a TNR is triggered (e.g., Shara 1981; Townsley & Bildsten 2005). The small ignition mass leads in turn to a small ejected mass and a rapid photometric evolution (i.e., a short t_2 time). In addition, the high accretion rate coupled with the small ignition mass leads to a short recurrence time. Thus, such systems are characteristic of the RNe.

Most studies of the fundamental properties of novae have involved Galactic systems, however these studies have been often complicated by the effects of extinction. This is particularly true for novae in the direction of the galactic center making the study of novae from different stellar populations (bulge and disk) notoriously difficult. On the other hand, the study of extragalactic novae avoids or minimizes these problems by allowing the study of novae from different populations in nearby, spatially-resolved spiral galaxies, or galaxies of different Hubble types, from late type spirals like M33 (Della Valle et al. 1994; Williams & Shafter 2004) and M51 (Mandel et al. 2023), to giant ellipticals in the Virgo cluster Pritchett & van den Bergh (1987); Curtin et al. (2015); Shafter et al. (2017); Shara et al. (2016, 2023).

The Andromeda Galaxy (M31), our closest neighbor galaxy at a distance of approximately 780 kpc (McConnachie et al. 2005), offers an unparalleled opportunity to study a large population of novae at a nearly uniform distance, mitigating the heavy extinction and distance uncertainties that complicate Galactic nova studies. It has been a cornerstone for nova studies going back to the pioneering work of Hubble and collaborators in the early 20th century (Hubble 1929). Since Richey discovered the first nova in M31 on 1909 September 13 (Richey 1917), over 1300 novae have been cataloged to date (e.g., see Shafter 2019; Della Valle & Izzo 2020a, and references therein). About half these novae have been discovered serendipitously as part of unrelated studies, or through the efforts of the increasing number of amateur astronomers who now routinely patrol the galaxy. The remaining half were discovered as part of a relatively small number of targeted nova surveys that continued after Hubble's initial survey (most notably Arp 1956; Rosino 1964, 1973; Ciardullo et al. 1987; Shafter & Irby 2001; Darnley et al. 2004; Rector et al. 2022). Taken together, these studies have established a nova rate of $\sim 50 \text{ yr}^{-1}$, which is comparable to estimates for the Milky Way (e.g. Shafter 2017; De et al. 2021; Kawash et al. 2022).

In addition to the determination of the nova rate, there have been several attempts to study the nova populations in M31. In an early study employing H α imaging (to provide better contrast against the bright background of M31's inner bulge) to discover 40 novae, Ciardullo et al. (1987) suggested that M31's nova population was dominated by the galaxy's bulge component. A little over a decade later Shafter & Irby (2001) confirmed these results with a similar study of 82 novae imaged in H α with the 40-in reflector at Mt Laguna Observatory.

A comprehensive study of M31's nova populations was presented by Shafter et al. (2011) who compiled broad-band photometric and spectroscopic data for a large sample of M31 novae. With the exception of a slight tendency for slower novae ($t_2 \lesssim 25 \text{ d}$) to be found closer to the center of M31, the study failed to find a significant dependence of nova properties (spectroscopic class and t_2 times) on spatial position, and hence stellar population in M31. A few years later, Shafter et al. (2015) studied the RN population of M31 and again found no evidence that the spatial distribution of the RN population differed from that of novae generally.

Despite the wealth of data on the observed behavior of M31 novae, very little is known about their fundamental properties such as their WD masses and accretion rates. On the other hand, despite the challenges alluded to earlier, tremendous progress has been made in recent years in our understanding of the fundamental properties of Galactic novae including their distances, luminosities and WD masses (e.g., Shara et al. 2018; Schaefer 2018; Selvelli & Gilmozzi 2019; Schaefer 2022, 2025).

In this paper we exploit the comprehensive and uniform sample of R -band light curves for the large sample of novae in M31 recently published by Clark et al. (2024) to explore for the first time the fundamental properties (WD masses, accretion rates, ejecta velocities, and predicted recurrence times) of novae in M31. Our analysis mirrors that for Galactic novae undertaken by Shara et al. (2018) where they estimated the masses of a large sample of novae using the extensive grid of nova models computed by Yaron et al. (2005). We conclude our study by comparing the fundamental properties and observed behavior of M31 novae with their counterparts in the Galaxy.

2. THE M31 LIGHT CURVE DATA

The R -band light curves from a large sample of M31 novae collected over two decades from 2002 to 2022 have recently been published by Clark et al. (2024). The novae were divided into three classes based upon their gross light-curve

morphology: “Linear” systems that exhibited essentially monotonic declines (84 novae), “Break” systems showing a discontinuous change in the slope of the decline (53 novae), and a “Jitter” class that included novae with relatively slow, fluctuating declines from maximum light (27 novae). In addition, known RNe were considered by Clark et al. as a separate class (17 eruptions from 13 nova progenitors). For all systems, the peak absolute magnitude in the R -band, M_R , and the rate of decline as characterized by the t_2 time were measured for a total of 177 M31 novae¹.

The large and homogeneous sample of novae from the Clark et al. study is unprecedented, and offers a unique opportunity to explore the fundamental properties of novae in M31. Here, we employ the nova models of Yaron et al. (2005) to estimate a range of nova properties including the mass and accretion rate of the WD, M_{WD} and \dot{M} , as well as the maximum ejection velocity, V_{max} and the expected recurrence time, P_{rec} for each nova in the sample.

3. NOVA MODELS

Yaron et al. (2005) have computed an extensive grid of nova models relating observable characteristics of the eruption to fundamental properties of the underlying progenitor binary. In particular, their Table 3 gives properties such as the bolometric luminosity at the peak of the eruption, L_4 (in units of $10^4 L_{\odot}$), the mass loss timescale, t_{ml} , the amplitude of the outburst, A , the maximum velocity of the ejecta, V_{max} , and the recurrence time between successive eruptions, P_{rec} , as functions of the WD mass, M_{WD} , accretion rate, \dot{M} , and core WD temperature, T_{WD} .

Our analysis follows a procedure similar to that adopted by Shara et al. (2018) in their determination of similar properties for a sample of Galactic novae. A key difference lies in the choice of the observational input parameters. In particular, Shara et al. (2018) used the eruption amplitude A ($\equiv m_{\text{min}} - m_{\text{max}}$) and the mass-loss timescale t_{ml} (taken as equivalent to the t_2 time). However, the eruption amplitude A is highly sensitive to the evolutionary state of the donor star (main-sequence or evolved), making its use problematic for many novae where the nature of the secondary star is unknown or uncertain. This is a fatal drawback in the case of novae in M31, where the nature of the secondary stars are almost all unknown, and the great distance makes even an estimate of the magnitude at minimum light, and thus A , unavailable for the vast majority of M31 novae. In place of the outburst amplitude, we substitute the peak bolometric luminosity, L_4 , which is available from a nova’s R -band absolute magnitude at maximum light, M_R , as an input parameter. The high luminosity of novae at the peak of eruption makes L_4 insensitive to the luminosity of the system at quiescence and thus to the nature of the secondary star. Then, following Shara et al. (2018), we also adopt the observed t_2 time as a proxy for t_{ml} , and assume $t_{\text{ml}} \equiv t_2$.

To estimate the bolometric magnitude of a nova from its absolute R -band magnitude requires us to specify the $V - R$ color and the bolometric correction of a typical nova at maximum light. We estimate the colors of our nova sample using results from the recent study by Craig et al. (2025) who find median colors of $B - V = 0.16$ mag and $V - R = 0.17$ mag for their recommended “Silver” sample of Galactic novae that were observed within 1 mag of peak brightness. To estimate the bolometric correction, we draw on the study by Pecaut & Mamajek (2013). From their Table 5 for the intrinsic colors, effective temperatures and bolometric corrections for 09 – M9 dwarfs, we find that $B - V \sim 0.16$ corresponds to an effective temperature of $T_{\text{eff,peak}} \sim 8000$ K, and a bolometric correction, $BC = -0.02$. Thus, our expression for the bolometric luminosity of a nova with absolute magnitude, M_R , at maximum light (in units of $10^4 L_{\odot}$) is given by:

$$L_4 = 10^{(-4 - 0.4[M_R + (V - R) + BC - M_{\text{bol},\odot}])}, \quad (1)$$

where $M_{\text{bol},\odot} = 4.74$ (Torres 2010), and we have adopted $V - R = 0.17$ (median of the Galactic nova sample) and $BC = -0.02$ (characteristic of main-sequence stars with $B - V = 0.17$). The uncertainty in the luminosity of a given nova, σ_{L_4} , has been determined by propagating the uncertainties in M_R and $V - R$. Specifically: $\sigma_{L_4} = 0.4 \ln(10) L_4 (\sigma_{M_R}^2 + \sigma_{(V-R)}^2)^{0.5}$.

3.1. Choice of T_{WD}

Another slight difference between our analysis and that of Shara et al. (2018) concerns the adopted value of T_{WD} , which must be specified for the Yaron et al. (2005) models. Specifically, the model grid is divided into three representative WD temperature regimes: $T_{\text{WD}} = 10, 30$, and 50×10^6 K thought to be appropriate for accreting WDs in nova binaries.

¹ One of these objects, M31N 2015-01a, is a rare Luminous Red Nova (Kurtenkov et al. 2015) that was mistakenly included in Clark et al. (2024). It has been replaced in the present study by the RN M31N 2017-01e omitted in Clark et al., keeping the total number of novae at 177.

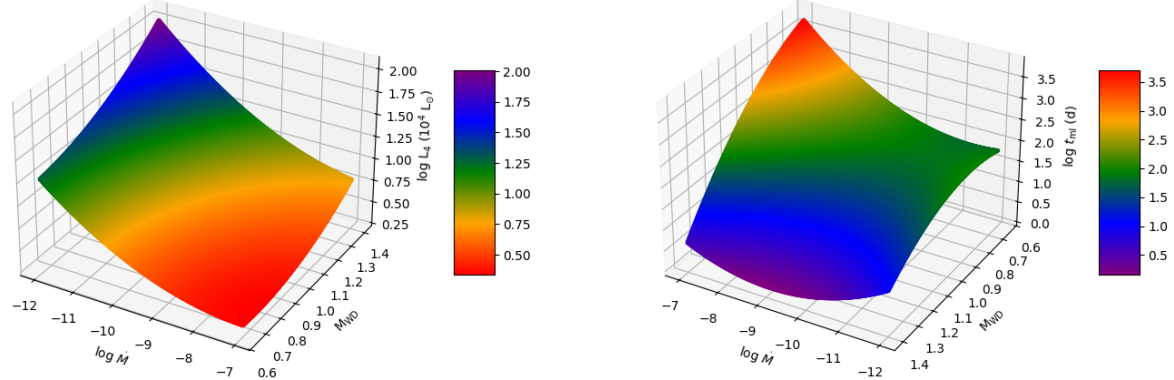


Figure 1. The interpolated model grids for our key input parameters, the bolometric luminosity at the peak of the eruption, L_4 , (left panel), and the mass-loss timescale, t_{ml} (Right Panel) as functions of $\log \dot{M}$ ($M_\odot \text{ yr}^{-1}$) and M_{WD} (M_\odot). The interpolation was performed by fitting second-order polynomials to the nova models of Yaron et al. (2005) as described in section 3.2.

The choice of the appropriate temperature is not immediately obvious. Steady-burning T_{WD} values ($\sim 5 - 8 \times 10^7 \text{ K}$) are too high given that the accretion rates \dot{M} ($\sim 10^{-11} \text{ to } 10^{-8} M_\odot \text{ yr}^{-1}$) are typically well below the critical rate for steady hydrogen burning (e.g., $\dot{M}_{\text{crit}} \sim 1 - 2 \times 10^{-7} M_\odot \text{ yr}^{-1}$ for a $1.0 M_\odot$ WD; Nomoto et al. 2007). In this regime, ^3He -driven limit cycles dominate, triggering premature thermonuclear runaways that prevent significant core heating (Townsley & Bildsten 2004).

In their Galactic nova study, Shara et al. (2018) arbitrarily adopted $T_{\text{WD}} = 30 \times 10^6 \text{ K}$, while noting that nova outburst models are relatively insensitive to the choice of T_{WD} . However, we selected the lower $T_{\text{WD}} = 10 \times 10^6 \text{ K}$ value for our analysis, motivated by Townsley & Bildsten (2004). In particular, their Figure 8 (upper panel) shows that for accretion rates $\log \dot{M}(M_\odot \text{ yr}^{-1}) \lesssim -8$ typical of nova systems, WD temperatures are expected to be $\lesssim 10 \times 10^6 \text{ K}$. Since our analysis focuses on $\log \dot{M}$ from -12.0 to -7.0 , the $T_{\text{WD}} = 10^7 \text{ K}$ models best match the physical conditions of nova outbursts in our study. The insensitivity of the models to T_{WD} noted by Shara et al. (2018), coupled with our own experimentation, suggests our results are robust despite our choice of the lower WD temperature.

3.2. Interpolation of the Model Grid

The model grid given in Table 3 of Yaron et al. (2005) is rather coarse, consistently spanning six values of $\log \dot{M}$ (from -12 to -7) for just four representative values of M_{WD} ($0.65, 1.00, 1.25, 1.40 M_\odot$). To enable high-resolution mapping between the observable quantities ($L_4, t_2, V_{\text{max}}, P_{\text{rec}}$) and the relevant physical parameters ($\log \dot{M}$ and M_{WD}), we have interpolated the $T_{\text{WD}} = 10 \times 10^6 \text{ K}$ model grid (reproduced in Table 1), using second-order polynomial surface fits similar to the approach taken by Shara et al. (2018). Specifically, for each model nova parameter Z (i.e., $L_4, t_{\text{ml}}, V_{\text{max}}, P_{\text{rec}}$), our interpolation model fits the following expression:

$$\log Z(X, Y) = c_1 + c_2 X + c_3 Y + c_4 X^2 + c_5 XY + c_6 Y^2, \quad (2)$$

where $X \equiv \log \dot{M}$ and $Y \equiv M_{\text{WD}}$. The coefficients c_1, \dots, c_6 are determined via least-squares minimization using the normal equations, solved with Gaussian elimination. The fit was performed in $\log Z$ to ensure positivity, and is appropriate for quantities spanning many orders of magnitude. The resulting interpolation was evaluated on a dense grid: 500 points in $\log \dot{M}$ ($\Delta X = 0.01$) and 750 points in M_{WD} ($\Delta Y = 0.001 M_\odot$), yielding a total of $N = 375,000$ interpolated points per model parameter. Where necessary (e.g., for $\log \dot{M} = -12; M_{\text{WD}} = 1.40$) to fill out the complete grid, the fit was extrapolated. The uncertainty in the model fit has been assessed by computing the typical residual error in $\log Z$ from the squared differences between observed and predicted values at the original grid points. This error is then propagated through the fit coefficients to estimate the standard error in $\log Z$ at any interpolated point.

The interpolated grids are shown in Figures 1 and 2.

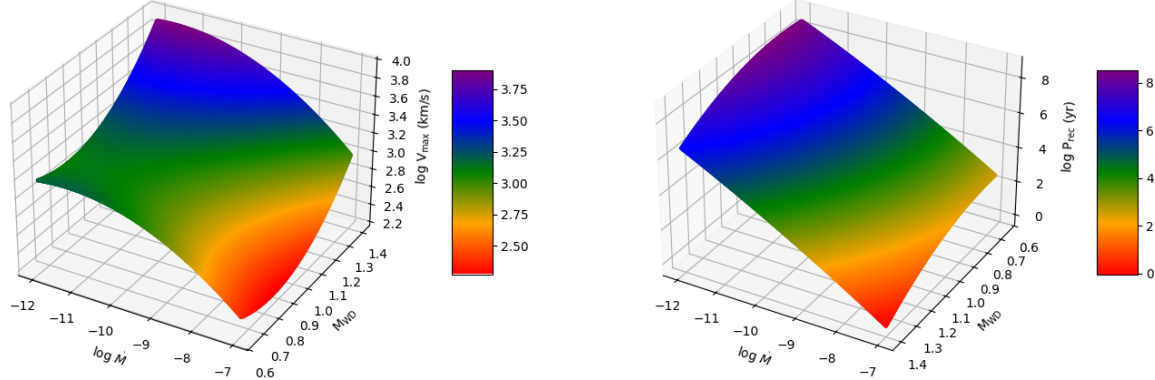


Figure 2. The same as in Fig. 1 except showing the model interpolations for the auxiliary parameters, the maximum expansion velocity of the nova ejecta, V_{\max} (left panel), and the predicted recurrence time, $\log P_{\text{rec}}$ (right panel).

4. GRID INVERSION AND DETERMINATION OF NOVA PARAMETERS

Log accretion rates (X) and WD masses (Y) have been estimated for each M31 nova by inverting the interpolated $L_4(X, Y)$ and $t_{\text{ml}}(X, Y)$ grids for the observed values of L_4 (through Eqn. 1) and the observed t_2 time, with observational uncertainties σ_{L_4} and σ_{t_2} and model interpolation uncertainties $\delta_{L_4,i}$ and $\delta_{t_{\text{ml}},i}$ at a given grid point i . The effective uncertainty in $L_{4,i}$ and $t_{\text{ml},i}$ at this grid point is then

$$\Delta_{L_{4,i}} = \sqrt{(\sigma_{L_4})^2 + \delta_{L_{4,i}}^2}, \quad \Delta_{t_{\text{ml},i}} = \sqrt{(\sigma_{t_2})^2 + \delta_{t_{\text{ml},i}}^2}. \quad (3)$$

The identification of the best estimates of $\log \dot{M}$ and M_{WD} begins by searching the grid for all points in an effective error box that simultaneously satisfies the following constraints:

$$|L_{4,i} - L_4| < \Delta_{L_{4,i}} \quad \text{and} \quad |t_{\text{ml},i} - t_2| < \Delta_{t_{\text{ml},i}}. \quad (4)$$

In rare cases where no points satisfied these criteria, the effective uncertainties ($\Delta_{L_{4,i}}$ and $\Delta_{t_{\text{ml},i}}$) were increased by incrementing the observational uncertainties (σ_{L_4} and σ_{t_2}) by their original values until a solution was found.

Once a set of potential solutions (an error box) for each nova were identified, the the best estimates of $\log \dot{M}$ and M_{WD} were found by minimizing the weighted Euclidean norm,

$$\chi_i = \sqrt{\left(\frac{L_{4,i} - L_4}{\Delta_{L_{4,i}}}\right)^2 + \left(\frac{t_{\text{ml},i} - t_2}{\Delta_{t_{\text{ml},i}}}\right)^2}, \quad (5)$$

for all points within the error box. The grid point i_{\min} corresponding to the smallest χ_i then provides our optimal solutions for the mass accretion rate and the WD mass, $\log \dot{M}(i_{\min})$ and $M_{\text{WD}}(i_{\min})$.

Uncertainties in the adopted values of $\log \dot{M}$ and M_{WD} have been estimated as the root-mean-square (RMS) deviations from the optimum value of all points satisfying our uncertainty constraints. This non-parametric RMS method measures the true spread of all acceptable solutions inside effective the error box, while accounting for how tightly or loosely the points cluster. The method works well even when the allowed region is long, narrow, or irregularly shaped. It gives more weight to solutions near the best fit, and it includes both observational errors and model interpolation uncertainties without assuming any specific error distribution. We have done our best to estimate uncertainties in our derived parameters given the available observational error estimates and model grid fit errors, but these estimates may not capture the full extent of the parameter uncertainties due to any unaccounted-for systematic errors.

4.1. Derived Quantities, V_{\max} and P_{rec}

For a given M31 nova in our sample, we are now in a position to predict the values of other potentially observable quantities such as the maximum velocity of its ejecta, as well as the likely interval between successive eruptions. Specifically, armed with the optimum solutions for the model parameters M_{WD} , $\log \dot{M}$, and their associated uncertainties, we have employed the interpolated model grids shown in Figure 2 to estimate the optimum values (and their uncertainties) for both V_{\max} and P_{rec} .

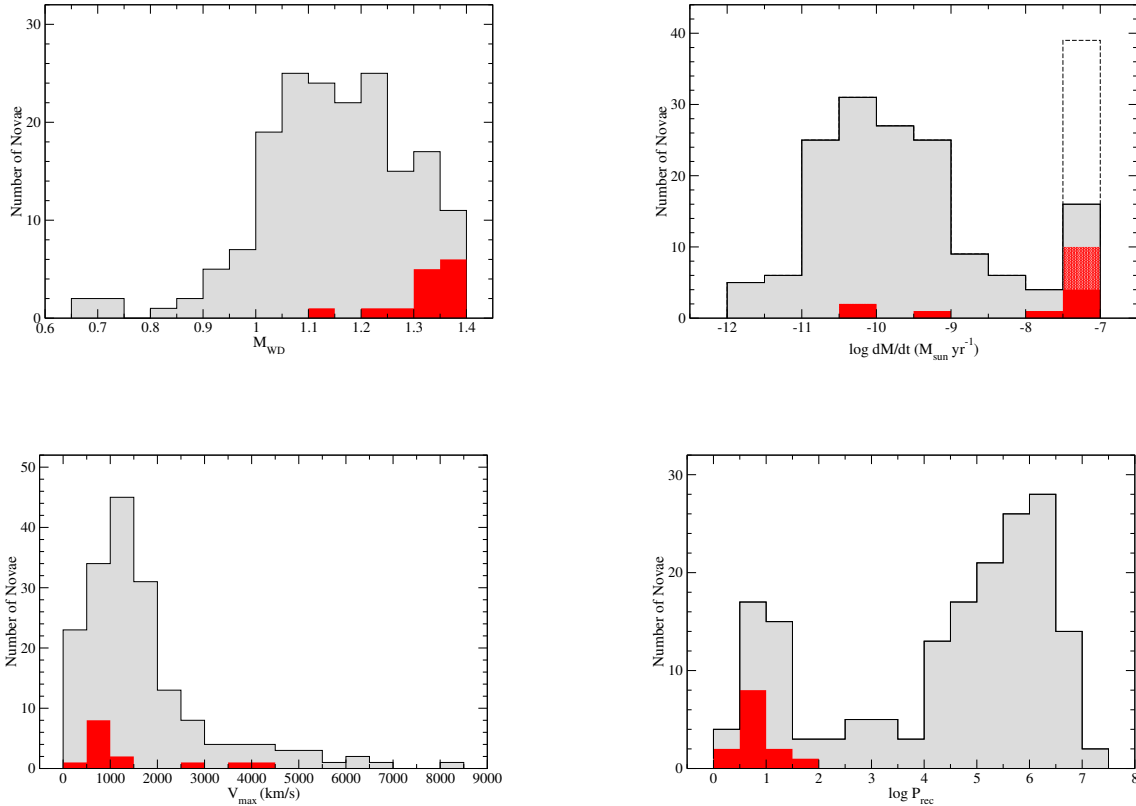


Figure 3. Distributions of the observed nova properties based on the model predictions from Tables 2 - 5. Top Left: The observed WD mass, M_{WD} , distribution (known RNe shown in red). Top Right: The mass accretion rate, $\log \dot{M}$, distribution. The dashed region in the brightest bin shows the contribution of all novae (RNe in light red), including those with uncertain estimates of $\log \dot{M} = -7.0$, while the grey and dark red regions omit these novae. Bottom Left: The maximum ejecta velocity, V_{max} , distribution (known RNe shown in red). Bottom Right: The recurrence time, $\log P_{\text{rec}}$, distribution. For known RNe, observed values of the recurrence times are shown.

5. OBSERVED DISTRIBUTIONS OF NOVA PARAMETERS

Our best estimates of M_{WD} , $\log \dot{M}$, V_{max} and P_{rec} for the M31 novae presented in Clark et al. (2024) are given in Tables 2 - 5, where for consistency we have maintained the distinction between the various light curve morphologies: Linear, Break, and Jitter, and considered the 14 known RNe with available light curve data separately. Available data for all 22 known and suspected M31 RNe are summarized in Appendix A. Finally, for completeness, we also have included in the tables values for the model input light curve parameters L_4 and t_2 , and retained the original quality assessment (Gold, Silver, Bronze) from Clark et al. (2024).

Figure 3 shows the observed distributions of WD mass, M_{WD} , mass accretion rate, $\log \dot{M}$, maximum ejection velocity, V_{max} , and recurrence times, $\log P_{\text{rec}}$, for our sample of 177 M31 novae. The mean values and the RMS errors for each observed distribution, light curve morphology and quality rating are summarized in Table 6. Generally, the distribution means are consistent across the various light curve morphologies and quality designations. Thus, for simplicity, we will only consider the properties of the aggregate sample of novae in the remaining discussion.

Each distribution is discussed in more detail below.

5.1. The WD mass distribution

The WD mass distribution is characterized by a mean of $1.15 M_{\odot}$ with an RMS deviation about the mean, $\text{RMSD}(M_{\text{WD}}) = 0.14$. Overall, the distribution appears to be very similar to that found by Shara et al. (2018)

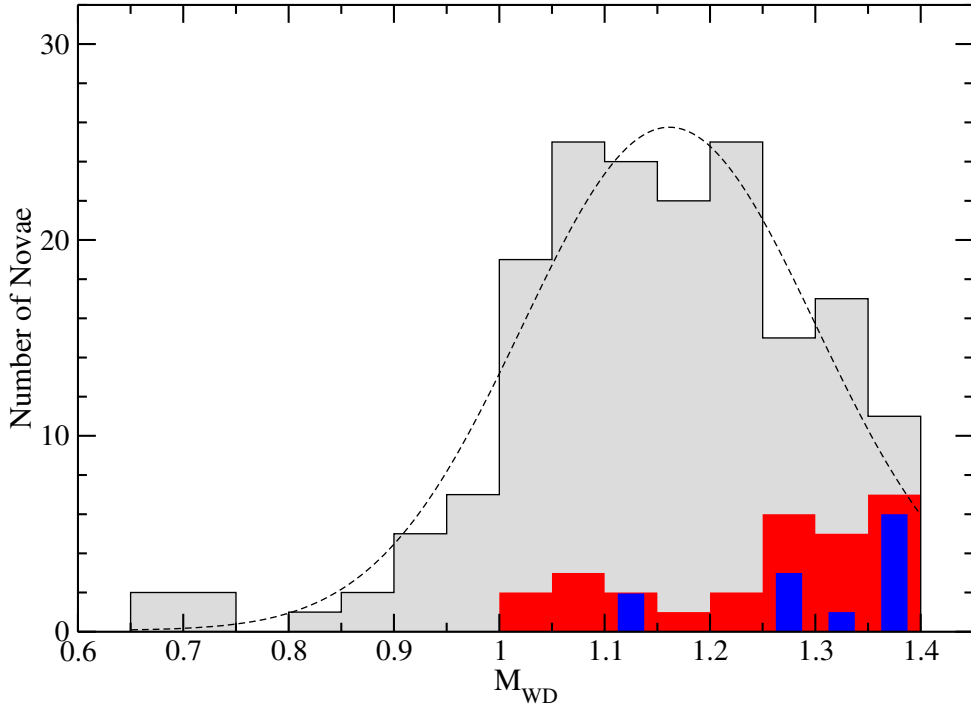


Figure 4. The observed distribution of the WD mass for He/N and Fe IIb M31 novae compared with the overall WD mass distribution. The red distribution show all known and suspected He/N and Fe IIb novae, while the blue distribution shows firmly established He/N novae. The average WD mass, $\langle M_{\text{WD}} \rangle = 1.15 \pm 0.14 M_{\odot}$, $1.26 \pm 0.12 M_{\odot}$, and $1.32 \pm 0.09 M_{\odot}$ for all novae, known and suspected He/N + Fe IIb novae, and firmly established He/N novae, respectively.

in their study of 82 Galactic novae, where they found the observed distribution of WD masses could be approximated by a Gaussian with a mean of $1.13 M_{\odot}$ and a FWHM = $0.29 M_{\odot}$ ($\sigma = 0.12$).

Not surprisingly, the known RNe in our M31 sample (shown in red) are strongly concentrated toward the right tail of the observed WD mass distribution, as is the case for Galactic novae. Models have consistently shown that massive WDs and relatively high accretion rates are necessary to produce recurrence times of order 100 yr, or less (e.g., Wolf et al. 2013; Kato et al. 2014).

The spectra of RN shortly after eruption usually exhibit broad Hydrogen Balmer, Helium (He I, He II), and Nitrogen (N II, N III) emission lines characteristic of the He/N spectroscopic class in the scheme of Williams (1992). To explore the dependence of spectroscopic class on WD mass, we have reproduced the observed WD mass distribution in Figure 4, showing where the He/N and broad-lined Fe II (Fe IIb) novae fall within the overall distribution. As expected, the He/N and Fe IIb novae, of which the RNe are a subset, are concentrated at higher mass. If we approximate the overall distribution by a Gaussian (dashed line, truncated at $1.4 M_{\odot}$) we find a mean of $\langle M_{\text{WD}} \rangle = 1.16$ and standard deviation, $\sigma = 0.14$, which are essentially identical to the sample mean and RMS deviation determined from the individual WD mass estimates.

5.2. The observed $\log \dot{M}$ distribution

The distribution for $\log \dot{M}$ is surprisingly bimodal with the main concentration of novae clustered around an estimated accretion rate of $\sim 10^{-10} M_{\odot} \text{ yr}^{-1}$. However, there is also a spike of novae with accretion rates near $10^{-7} M_{\odot} \text{ yr}^{-1}$, where the majority of the RNe are found. The excess of novae at the high end of the accretion rate distribution possibly results from truncation of the model grid, which does not extend to accretion rates above $\log \dot{M} = -7$. As

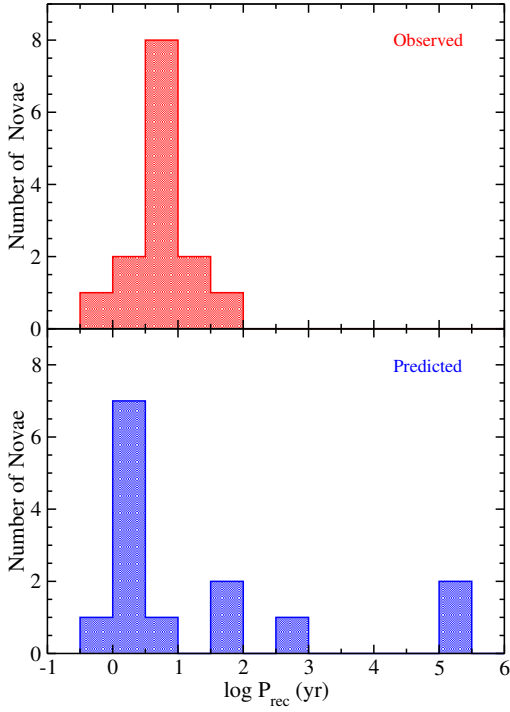


Figure 5. The observed distribution of the RN recurrence times (top panel) compared with the predicted RN recurrence time distribution based on the model fits (bottom panel). The model fails to accurately predict the recurrence times for three RNe (M31N 1984-07a, 2006-11c, 2013-10c).

a result, the best-fit solutions for any novae accreting at rates higher than this will accumulate at this end of the distribution. Novae falling at the edge of the grid with accretion rate estimates of exactly $\log \dot{M} = -7$ (indicating that the true values may lie above this accretion rate) are marked as uncertain in Tables 2 – 5 and are represented by the unshaded portion of the histogram. Not coincidentally, a significant fraction of these novae turned out to be ones that failed to converge using the initial error estimates during the grid inversion process. In these cases, convergence was achieved only after incrementing the initial values of the error estimates for L_4 and t_2 . It is therefore reasonable to assume that the derived $\log \dot{M}$ values for these systems are particularly uncertain. It is also possible that many of these systems are unrecognized RN systems with evolved secondary stars producing high accretion rates.

5.3. The predicted V_{\max} distribution

The distribution for the predicted maximum ejecta velocity is characterized by a strong peak between 1000 and 1500 km s⁻¹. This is typical of the FWHM of the Balmer emission lines seen in the vast majority of novae, most of which are members of the Fe II spectroscopic class (Williams 1992). Surprisingly, the distribution of the maximum expansion velocities for known RNe generally follows that of the overall nova distribution, which is dominated by relatively narrow-lined Fe II novae. However, as mentioned earlier, most recurrent novae are members of the He/N class with emission lines typically characterized by FWHM $\gtrsim 2500$ km s⁻¹. The root of this discrepancy can be traced back to the model grid for V_{\max} (see Fig 2, left panel). Expansion velocities in excess of 2000 km s⁻¹ can only be produced for high mass WDs accreting at rates $\dot{M} \lesssim 10^{-8} M_{\odot}$ yr⁻¹, whereas most RNe have accretion rates $\sim 10^{-7} M_{\odot}$ yr⁻¹.

5.4. The predicted recurrence time distribution

As with the observed $\log \dot{M}$ distribution, the distribution for the predicted recurrence times is also bimodal, with one peak near a recurrence time of ~ 10 yr, and the other at considerably longer intervals of order several $\times 10^5$ yr. All

of the novae in the former group with $P_{\text{rec}} < 100$ yr are either known or unrecognized RNe. It is tempting to speculate that the bimodal nature of the distribution results from differences in the evolutionary state of the mass donor, and that the peak at recurrence times ~ 10 yr is formed by systems harboring evolved secondary stars.

Given that the true recurrence times (or possibly upper limits in some cases) are known for the RN sample offers an opportunity to check the predictive power of the models themselves. Figure 5 shows the distributions of the observed recurrence times compared with the model predictions. For the majority of known RN, the models correctly assign recurrence times, $P_{\text{rec}} \lesssim 100$ yr. However, for four of the 17 observed RNe eruptions (M31N 2012-09a, 2013-10c, 2015-02b, and 2022-11b) the predicted recurrence times are considerably longer. The two eruptions with the longest predicted recurrence times (2012-09a and 2022-11b) are believed to be subsequent eruptions of M31N 1984-07a. This nova appears very close to the nucleus of M31 making it difficult to firmly establish that the novae arise from the same progenitor. It is therefore possible, although unlikely, that the object may not be a RN, but instead the chance positional near-coincidence of three unrelated novae (see the discussion in Shafter et al. 2015) for further details. The other two RN eruptions occur further from the nucleus of M31, and the RN designations are thus much more secure. In all cases, the Yaron et al. (2005) models require accretion rates $\lesssim 10^{-9} M_{\odot} \text{ yr}^{-1}$ to achieve the relatively high luminosity of the observed eruptions ($M_R < -8$). In such systems, the recurrence times are predicted to be $\gtrsim 500$ yrs even for the most massive WDs.

6. INTRINSIC DISTRIBUTIONS FOR M_{WD} AND $\log \dot{M}$

As emphasized by Shara et al. (2018) in their study of the Galactic nova population, the observed distributions of M_{WD} and $\log \dot{M}$ are strongly biased toward systems with short recurrence times. Given our estimates of P_{rec} for the individual novae, it is straightforward to estimate the intrinsic (unbiased) mean for the M_{WD} and $\log \dot{M}$ distributions by simply weighting the observed values of the WD mass, $M_{\text{WD},i}$, and log accretion rate, $[\log \dot{M}]_i$, by P_{rec} . Specifically, for recurrence time weights $w_{\text{rec},i} = P_{\text{rec},i} / \sum_{i=1}^N P_{\text{rec},i}$, we have: $\langle M_{\text{WD}} \rangle_{\text{int}} = \sum_{i=1}^N w_{\text{rec},i} M_{\text{WD},i}$ and $\langle \log \dot{M} \rangle_{\text{int}} = \sum_{i=1}^N w_{\text{rec},i} [\log \dot{M}]_i$. When applied to the full sample of $N = 177$ novae in Tables 2 – 5 we find $\langle M_{\text{WD}} \rangle_{\text{int}} = 1.07 M_{\odot}$, and $\langle \dot{M} \rangle_{\text{int}} = 2 \times 10^{-11} M_{\odot} \text{ yr}^{-1}$.

To determine the intrinsic distributions for M_{WD} and $\log \dot{M}$, we follow the procedure outlined in section 5 of Shara et al. (2018). Briefly, if the distribution of WD masses are divided into n_i bins, x_i , and the distribution of $\log \dot{M}$ values are divided into n_j bins, y_j , where $P_{x,\text{obs}}(x_i)$ is the observed fraction novae in WD mass bin x_i and $P_{y,\text{obs}}(y_j)$ is the observed fraction novae in $\log \dot{M}$ bin y_j , then the intrinsic fraction of novae in each WD mass and $\log \dot{M}$ bin is given by:

$$\begin{aligned} P_{x,\text{int}}(x_i) &= P_{x,\text{obs}}(x_i) \left[\sum_{j=1}^{n_j} \frac{P_{y,\text{obs}}(y_j)}{P_{\text{rec}}(x_i, y_j)} \right]^{-1} \\ P_{y,\text{int}}(y_j) &= P_{y,\text{obs}}(y_j) \left[\sum_{i=1}^{n_i} \frac{P_{x,\text{obs}}(x_i)}{P_{\text{rec}}(x_i, y_j)} \right]^{-1}, \end{aligned} \quad (6)$$

where the weighting function $P_{\text{rec}}(x_i, y_j)$ is obtained from the model interpolation for the recurrence time shown in the right panel of Figure 2.

The resulting intrinsic distributions, normalized to $\sum_{x_i=1}^{n_i} P_{x,\text{int}}(x_i) = \sum_{j=1}^{n_j} P_{y,\text{int}}(y_j) = N$, are shown in Figure 6. The means of the distributions are given by $\langle M_{\text{WD}} \rangle_{\text{dist}} = 1.01 M_{\odot}$ and $\langle \dot{M} \rangle_{\text{dist}} = 8 \times 10^{-12} M_{\odot} \text{ yr}^{-1}$. The mean of the WD mass distribution is close to that found in the direct recurrence-time-weighted average of the individual M31 novae, as well as to the true M_{WD} mean computed by Shara et al. (2018) for the Galactic novae. On the other hand, the intrinsic accretion rate mean for M31 novae is about an order of magnitude lower than the corresponding Galactic determination. The source of the discrepancy is unclear, but may possibly be related to the choice of nova amplitude, rather than peak luminosity, as a model input. The amplitude is quite sensitive to both the mass accretion rate (which determines the quiescent luminosity) and the evolutionary state of the secondary star. For systems with luminous secondaries, the eruption amplitudes will be reduced, resulting in an increase in the inferred accretion rates. Regardless of whether our M31 \dot{M} distribution can be brought in line with the Shara et al.'s Galactic distribution, the mass accretion rates remain surprisingly low and the recurrence times surprisingly long.

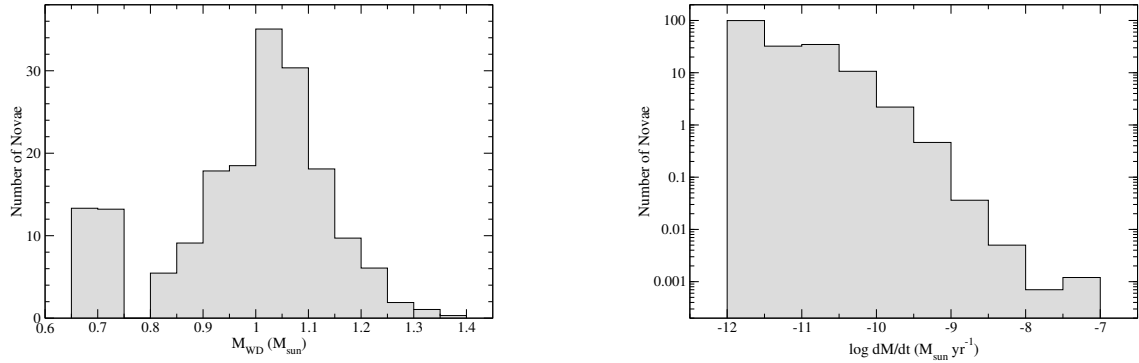


Figure 6. The intrinsic distributions of the WD mass (left panel) and $\log \dot{M}$ (right panel). The mean of the WD mass distribution is $\langle M_{\text{WD}} \rangle_{\text{dist}} = 1.01 M_{\odot}$, while that for the $\log \dot{M}$ distribution (shown as log number of novae for clarity) is given by $\langle \log \dot{M} \rangle_{\text{dist}} = -11.1$, corresponding to $\langle \dot{M} \rangle_{\text{dist}} = 8 \times 10^{-12} M_{\odot} \text{ yr}^{-1}$. The underlying nova population is dominated by systems with accretion rates $\lesssim 10^{-10} M_{\odot} \text{ yr}^{-1}$.

6.1. Evidence for Hibernation

Our analysis reveals an M31 nova population characterized by a high average WD mass ($\langle M_{\text{WD}} \rangle \approx 1.15 M_{\odot}$), a low average accretion rate ($\langle \dot{M} \rangle \approx 10^{-10} M_{\odot} \text{ yr}^{-1}$), and long average recurrence times ($\langle P_{\text{rec}} \rangle \approx 10^6 \text{ yrs}$). This result is internally consistent with the physics underlying TNR models (e.g., [Townsley & Bildsten 2005](#); [Wolf et al. 2013](#)), which show that this low average accretion rate forces the system to accumulate a large ignition mass ($M_{\text{ign}} \approx 10^{-4} M_{\odot}$) prior to the next eruption. This large ignition mass coupled with low accretion rates results in the long predicted recurrence times, P_{rec} ($\equiv M_{\text{ign}}/\dot{M}$).

The low derived accretion rates ($\dot{M} \lesssim 10^{-10} M_{\odot} \text{ yr}^{-1}$) directly conflicts with secular evolution models for cataclysmic variables (e.g., [Rappaport et al. 1983](#); [Knigge 2011](#); [Zorotovic & Schreiber 2020](#)), which predict much higher cycle-averaged nova accretion rates ($\sim 10^{-9}$ to $10^{-8} M_{\odot} \text{ yr}^{-1}$) driven by standard angular momentum loss mechanisms. The irradiation-driven hibernation hypothesis originally proposed by M. Shara four decades ago ([Shara et al. 1986](#); [Hillman et al. 2020](#)) provides the physical mechanism to bridge this gap. Following each eruption, strong irradiation of the secondary star by the hot white dwarf can force the secondary star out of thermal equilibrium and temporarily drive high mass transfer ($\sim 10^{-8} - 10^{-7} M_{\odot} \text{ yr}^{-1}$) for of order $\sim 10^2 - 10^3 \text{ yr}$. As the white dwarf cools, the irradiation fades and the secondary contracts toward its equilibrium radius, causing the accretion rate to drop to $\lesssim 10^{-11} M_{\odot} \text{ yr}^{-1}$ for the remainder of a prolonged ($\sim 10^5 - 10^6 \text{ yr}$) inter-outburst period. Thus, the low average accretion rates we derive from the [Yaron et al. \(2005\)](#) models reflects the system's dominant physical state: a prolonged ($\sim 10^6 \text{ yr}$) low-accretion hibernation tail ($\lesssim 10^{-10} M_{\odot} \text{ yr}^{-1}$) following the brief post-nova high state.

7. THE EFFECT OF STELLAR POPULATION

One of the unresolved questions in nova studies concerns whether observed properties (and thus the fundamental properties of the progenitor binary) vary systematically with changes in the underlying stellar population. Two observational characteristics that are expected to be particularly sensitive to stellar population are: (1) the average speed class, as measured by the t_2 time, and (2) the dominant spectroscopic class of the nova population (e.g., Fe II or He/N), as introduced by [Williams \(1992\)](#). Studies of Galactic novae have suggested that so-called “disk novae” (novae close to the Galactic plane) are faster and brighter than are “bulge novae” (novae observed further from the plane) (e.g., see [Della Valle & Izzo 2020b](#); [Cohen et al. 2025](#), and references therein). Convincing arguments have also been put forward that the traditional spectroscopic class of a nova (see [Williams 1992](#)) varies with stellar population in the Galaxy ([Della Valle & Livio 1998](#)).

The justification for the variation of speed class comes directly from models of TNRs on WDs which demonstrate that for a given accretion rate massive WDs have lower ignition masses (e.g., [Townsley & Bildsten 2005](#)). Under the assumption that the ejected masses are proportional to the ignition mass, novae with massive WDs will produce lower mass ejecta that rapidly become optically thin, leading to a faster photometric evolution.

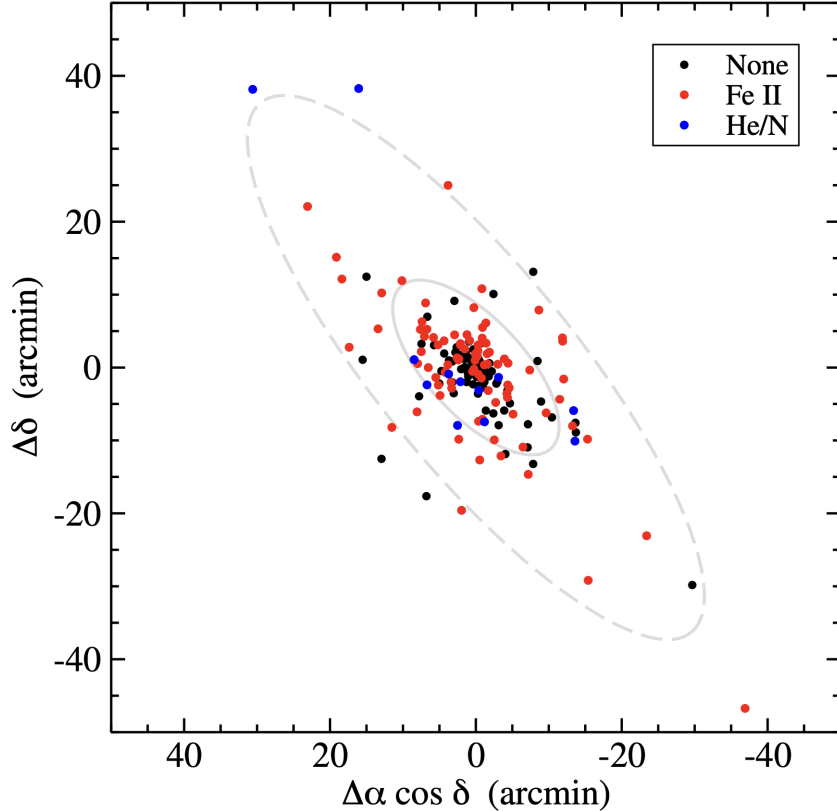


Figure 7. The spatial distribution of the 177 novae in our M31 sample (black filled circles). Known Fe II novae are shown in red, while firmly-established He/N novae are shown in blue. The solid and dashed grey contours show the $a = 15'$ and $a = 50'$ R -band isophotes, respectively. The majority of novae in our sample are part of M31’s bulge population.

The physics underlying the formation of novae with differing spectroscopic class is less well understood. Indeed, the very notion that a nova belongs to a given spectroscopic class has been called into question (Aydi et al. 2024). These authors present compelling evidence showing that the spectral evolution many Galactic novae display both Fe II and He/N lines at various times, and thus appear to transition between spectroscopic classes on the declining branch of their eruptions. This is no doubt the case, but it remains true that the line widths, in particular, shortly after maximum light appear to be markedly different in the classic He/N novae compared with the relatively narrow-lines and P-Cygni profiles that characterize their Fe II counterparts. That said, clearly the concept of spectroscopic classes of novae needs to be refined going forward.

7.1. The unique role of M31

As a nearby and spatially-resolved galaxy, M31 has played a key role in the study of nova populations. In their comprehensive study of the spectroscopic and photometric properties of novae in M31, Shafter et al. (2011) looked at the spatial distribution of a large sample of 91 M31 novae with spectroscopic data sufficient for classification and found no significant variation of spectroscopic class (Fe II vs He/N) with distance from the center of the galaxy as measured by the R -band isophotal radius. In light of the Galactic studies, this is perhaps surprising given that novae far from the center of M31 arise overwhelmingly from the galaxy’s disk population. Shafter et al. (2011) did however find a weak dependence of a nova’s rate of decline from maximum light – the t_2 time – with distance from the center of M31, in the sense that the “faster” novae ($t_2 \leq 25$ d) were slightly more spatially extended compared with their slower counterparts with t_2 values longer than 25 d.

We are now in a position to re-visit the photometric analysis using our updated sample of 177 M31 nova light curves, of which 143 are new (post 2009) and were not included in the analysis presented in Shafter et al. (2011). Figure 7 shows the spatial distribution of the novae in our M31 sample. The spectral types are indicated (red points: Fe II and blue points: He/N) when known. The inner isophote has a semimajor axis, $a = 15'$, which at the distance of M31 corresponds to a radius of $R \simeq 3.4$ kpc – slightly larger than the radius of M31’s bulge component. Novae outside

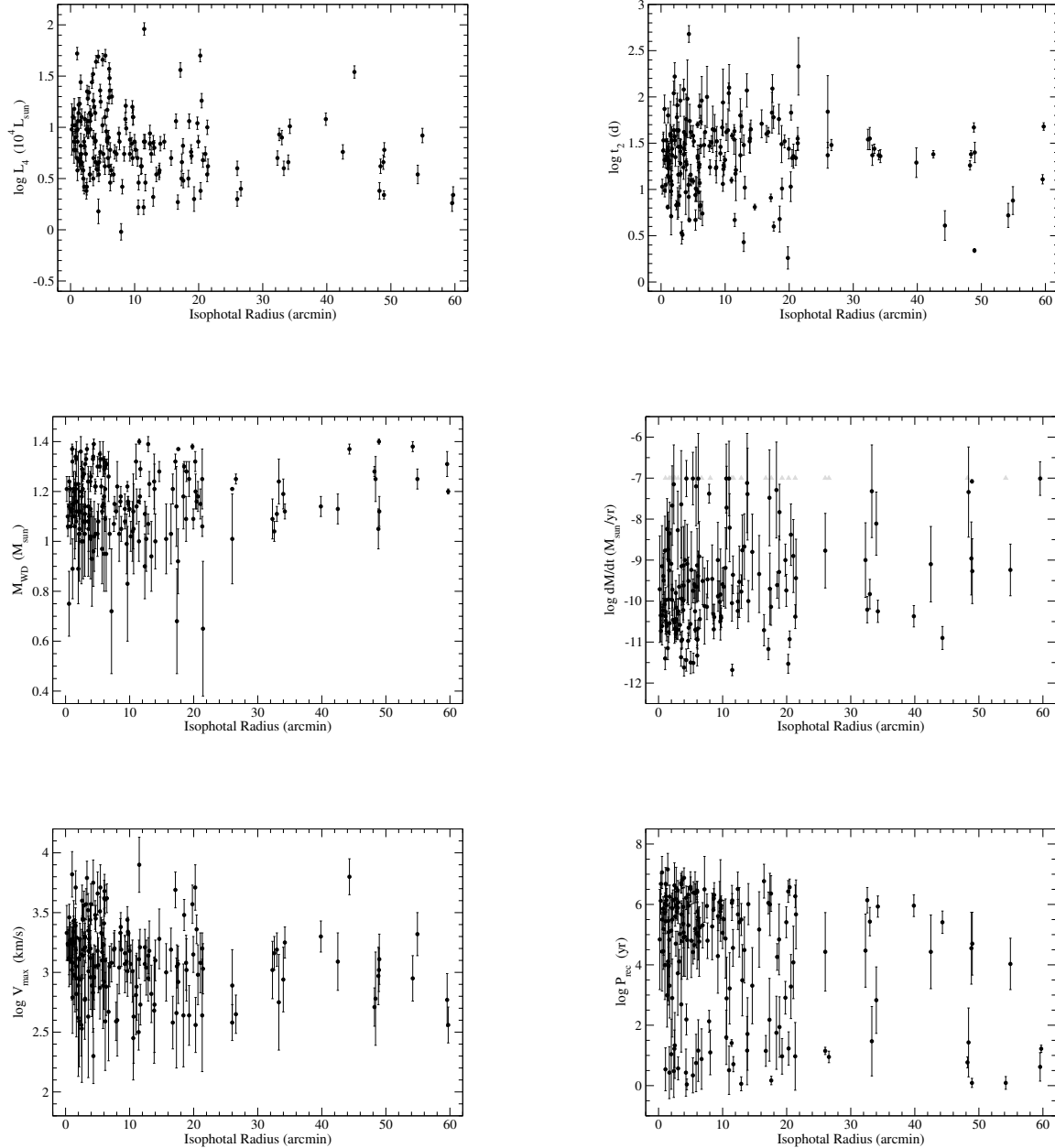


Figure 8. Dependence of nova properties on the isophotal radius, a , within M31. Top left: The peak luminosity, L_4 ; Top right: The t_2 time; Middle left: The observed WD mass, M_{WD} ; Middle right: the accretion rate, $\log \dot{M}$. The grey upward pointing triangles represent novae with $\log \dot{M} = -7$, which we consider lower limits on the true accretion rates; Bottom left: The maximum ejecta velocity, V_{max} ; Bottom right: The predicted recurrence time, $\log P_{\text{rec}}$. None of the observed properties show an obvious dependence on isophotal radius.

this radius are assumed to arise from M31's disk population. The observed spatial distribution does not accurately reflect the true spatial distribution of M31 novae because our observed sample is biased by more frequent observations of the inner bulge regions of M31. Thus, the relative number of novae with $a < 15'$ and novae with $a > 15'$ does not reflect the true ratio of bulge to disk novae. Nevertheless, despite the limited number of novae that are unambiguously from M31's disk, it is still possible to explore whether there are any obvious differences between the speed classes and spectral types of the bulge and disk novae in our sample.

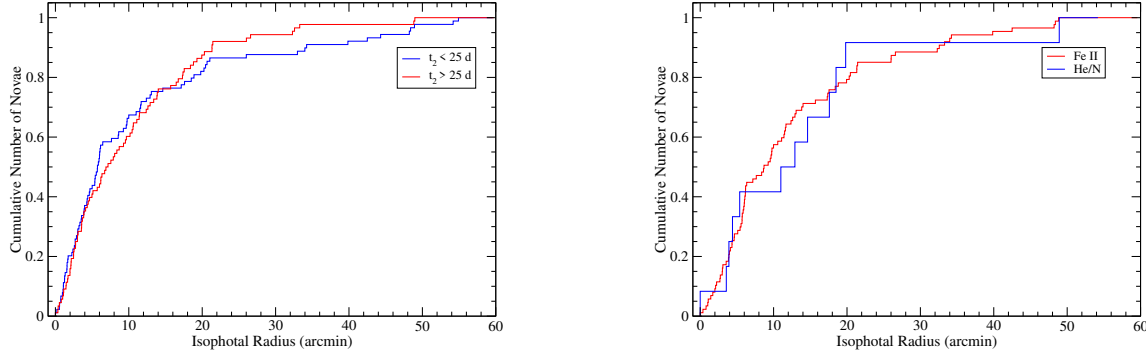


Figure 9. Left panel: The cumulative distributions of the isophotal radius, a , for novae with $t_2 \leq 25$ d (blue line) compared with novae with $t_2 > 25$ d (red line). A Kolmogorov-Smirnov test yields K-S statistic of K-S $p = 0.54$ demonstrating that there is no significant difference between the two distributions. Right panel: The cumulative distributions of the isophotal radius for novae belonging to the He/N spectroscopic class (blue line) compared with Fe II novae (red line). A K-S test yields $p = 0.86$ demonstrating that there is no significant difference between the two distributions.

Figure 8 shows the full slate of nova parameters plotted as a function of the isophotal radius, a . In addition to the derived nova parameters (M_{WD} , $\log \dot{M}$, V_{max} , and P_{rec}), we have also included the principal input parameters, L_4 and t_2 . None of the parameters show an obvious trend with distance from the nucleus of M31. However, we can test this impression by comparing the means for each parameter in the bulge and disk regions of M31 separately. Although the high inclination of M31 to our line of sight makes it difficult to unambiguously separate the bulge and disk components, if we assume that M31’s bulge and disk components dominate at isophotal radii, $a \leq 15'$ and $a > 15'$, respectively, we find no evidence that the t_2 time or M_{WD} vary with a . However, the mean values for the remaining parameters appear to differ at the $> 2\sigma$ level (see Table 7). In particular, there is a hint that the bulge novae may on average have marginally higher peak luminosities and accretion rates and longer recurrence times compared with novae with $a > 15'$ that we associate with the disk of M31. These results must be viewed with extreme caution, however, as all or part of this difference could result from our somewhat arbitrary choice of $a = 15'$ to divide the bulge and disk populations, or from other systematic effects that we have been unable to take into account, such as the spatial variation of extinction within M31.

A better approach for analyzing spatial variation of nova properties, such as speed and spectroscopic class, is to compare their cumulative distributions as functions of isophotal radius. Figure 9 shows cumulative distributions for both the speed class (“fast” vs. “slow”) and the spectroscopic class (He/N vs. Fe II) for the total of 116 novae in our sample for which it is known. Specifically, in the left panel we show the cumulative distributions of novae with $t_2 \leq 25$ d, which following Warner (2003) we refer to as “fast novae”, compared with novae characterized by $t_2 > 25$ d (here referred to as “slow novae”). The blue line shows the distribution for 93 objects in our “fast” sample while the red line shows the distribution for the remaining 87 “slow” novae. A Kolmogorov-Smirnov (K-S) test yields a K-S statistic $p = 0.55$, indicating that there is no significant difference between the two nova samples.

The right panel of Figure 9 shows the cumulative distributions for novae with known spectroscopic class. As with the speed class, a K-S test confirms that there is no significant difference between the spatial distributions of the 87 Fe II and 29 He/N novae in our sample.

Below we probe the stellar population of novae by comparing the aggregate properties of novae in M31 with their Galactic counterparts.

7.2. Comparison with the Galaxy

The Andromeda Galaxy (M31) is classified as SA(s)b (de Vaucouleurs et al. 1991), with a prominent classical bulge and tightly wound arms. In contrast, the Milky Way is classified as SAB(rs)bc (Bland-Hawthorn & Gerhard 2016), featuring a bar-driven pseudo-bulge and fragmented spiral arms. These structural differences, coupled with divergent star formation rate (SFR) histories can affect the present rates of novae and their observed properties.

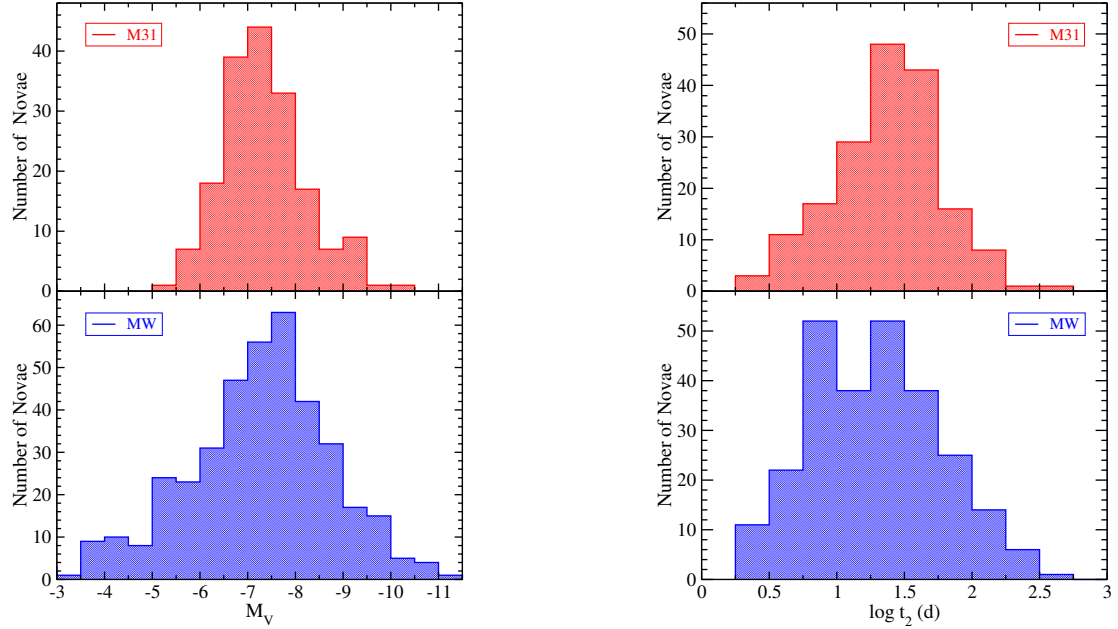


Figure 10. Left panel: The absolute magnitude at maximum light, M_V , for our M31 nova sample (red histogram) compared with the Galactic nova sample (blue histogram) of Schaefer (2025). Despite the low luminosity tail seen in the Galactic distribution, the absolute magnitude distributions of M31 and Galactic novae are remarkably similar. Right panel: The distribution of t_2 times for our M31 nova sample (M_R , red histogram) compared with the Galactic nova sample (M_V , blue histogram) from Schaefer (2025). There is no significant difference in the means for the two distributions.

As pointed out nearly three decades ago by Yungelson et al. (1997), stellar populations with more recent star formation are expected to produce a higher frequency of nova eruptions. This is primarily a consequence of the fact that the average mass of the WDs in *active* nova systems is expected to decline with time since the formation of the progenitor binary. The progenitor binaries containing massive WDs that formed long ago in older stellar populations have by now evolved to states with very low mass transfer rates and no longer contribute significantly to the active nova population (i.e., the recurrence times become extremely long). On the other hand, populations with more recent star formation are expected to be dominated by active novae containing more massive WDs, leading to eruptions that are on average brighter, faster, with shorter recurrence times compared with older stellar populations.

M31's current SFR is $\sim 0.25 M_\odot \text{ yr}^{-1}$ (Ford et al. 2013), largely confined to a 10 kpc ring that may have been triggered $\sim 100 - 200$ Myr ago from an interaction with its dwarf elliptical companion, M32 (Williams et al. 2015). The Milky Way has a significantly higher SFR of $\sim 1.7 M_\odot \text{ yr}^{-1}$, which is distributed across the disk (Licquia & Newman 2015). M31's star formation peaked 8 – 10 Gyr ago, yielding an older mean stellar age, while the Milky Way's more extended SF history has produced younger populations. In view of these differences, one can expect the nova rate per unit mass in stars to be higher in the Galaxy compared with M31, and to contain, on average, brighter and faster novae.

Current estimates of the nova rate in M31 range from $R_{\text{M31}} = 40 \text{ yr}^{-1}$ (Rector et al. 2022) to $R_{\text{M31}} = 65 \text{ yr}^{-1}$ (Darnley et al. 2006), while the most recent Galactic nova rate estimates have mostly fallen in the range of $R_{\text{MW}} \sim 40 - 50 \text{ yr}^{-1}$ (Shafter 2017; De et al. 2021; Kawash et al. 2022). To first order, given the uncertainties, the best estimates of the nova rates in M31 and the Galaxy appear to be comparable at a rate of $\sim 50 \pm 15 \text{ yr}$. On the other hand, estimates of the mass (in stars) of the two galaxies are significantly different, with M31 containing $\sim 1.5 - 2$ times the stellar mass of the Galaxy (Sick et al. 2015; Licquia & Newman 2015). Thus, M31 apparently has a lower nova rate per unit mass in stars, in agreement with the expectations for a relatively quiescent galaxy with relatively little recent star formation.

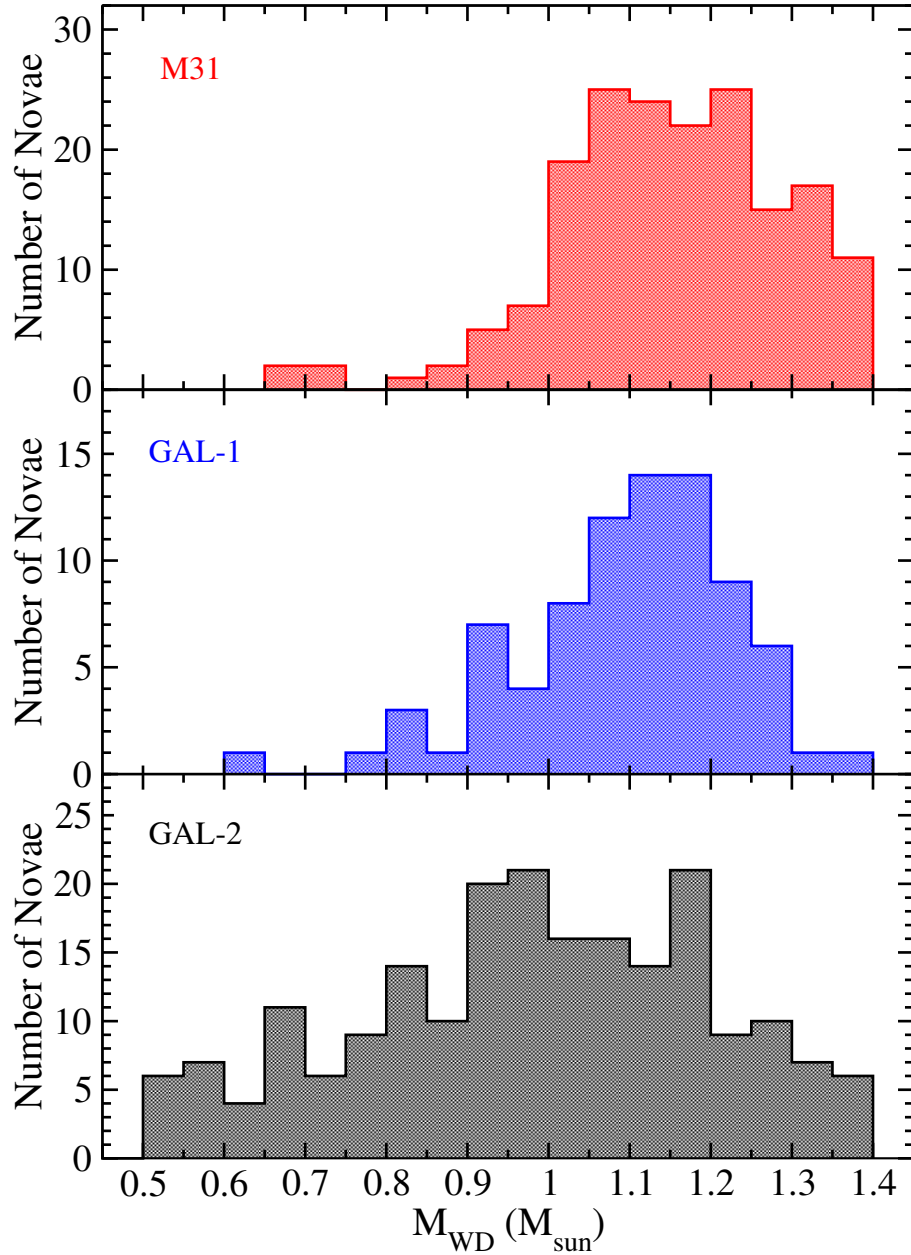


Figure 11. The distribution of apparent WD masses (uncorrected for recurrence time) from our M31 sample (top panel) compared with the Galactic nova samples of Shara et al. (2018) and Schaefer (2025). The M31 and Galactic sample from Shara et al. (2018) are similar with mean WD masses of $1.16 M_{\odot}$ and $1.13 M_{\odot}$, respectively; however, both of these distributions differ from that of Schaefer (2025) who finds a significantly lower mean WD mass for Galactic novae of $\sim 1 M_{\odot}$.

In addition to considering the overall nova rates, we can also compare the observed and model parameters of the nova populations in M31 and the Milky Way. Figure 10 shows a comparison of the V -band absolute magnitudes² from our M31 nova sample compared with that from the recent Galactic study by Schaefer (2025). With the exception of the faint tail (which, if present, would not be detected in our M31 survey), the two distributions appear similar. Indeed, if we only consider novae brighter than $M_V = -5$ we find $\langle M_V \rangle = -7.49 \pm 0.0653$ and $\langle M_V \rangle = -7.38 \pm 0.0659$, for the Galactic and M31 samples, respectively, which differ only at the $\sim 1\sigma$ level³. However, if we restrict the comparison to novae with $M_V < 6.0$, where we expect our M31 sample to be mostly complete, we find $\langle M_V \rangle = -7.78 \pm 0.0588$ for the Galactic sample, which is significantly brighter (at $> 3\sigma$) than the mean of our M31 nova sample, $\langle M_V \rangle = -7.46 \pm 0.0632$, in agreement with expectations based on the differences in stellar population.

We can also compare the rates of decline (t_2 times) between the same M31 and Galactic nova samples, as shown in the right panel of Figure 10. The mean of the M31 $\log t_2$ distribution is $\langle \log t_2 \rangle = 1.37 \pm 0.030$, while that for the Galactic sample is $\langle \log t_2 \rangle = 1.28 \pm 0.030$. Although the mean of the M31 $\log t_2$ distribution is slightly greater than that for the Galactic distribution, as expected if the M31 novae were on average “slower” than their Galactic counterparts, the difference is barely significant ($\sim 2.1\sigma$).

Now that the distribution of WD masses for a large sample of M31 novae is available, it is possible for the first time to directly compare the observed WD mass distributions for M31 and the Galaxy. Figure 11 shows the apparent M31 WD mass distribution along with the Galactic distributions from the work of Shara et al. (2018) and Schaefer (2025). As previously noted, the M31 WD mass distribution is remarkably similar to that determined by Shara et al. (2018) for the Galaxy. Although the apparent distributions (uncorrected for recurrence time bias) are shown here, the intrinsic distributions for M31 and the Galaxy also have very similar means and dispersions. The Galactic WD mass distribution based on the data from Schaefer (2025) is broader than that observed in M31, with a more prominent left tail towards lower WD masses. As noted by Schaefer in his discussion of the Shara masses, the source of the discrepancy – whether it lies with the Galactic nova data, or with the nova models, or both – is unclear.

8. CONCLUSIONS

We have analyzed the R -band light curves for a large and homogeneous sample of 177 novae in M31 using the Yaron et al. (2005) models to estimate fundamental properties of the progenitor binaries. To test for possible dependencies on stellar population, we explored whether any of the resulting nova properties, including the peak luminosity, rate of decline, WD mass, accretion rate, maximum ejection velocity, and recurrence time, varied systematically with deprojected distance (isophotal radius) from the center of M31. Finally, the properties of our M31 nova sample were compared with those for the Galactic nova population. Our principal conclusions can be summarized as follows:

(1) The observed distribution of WD masses in M31 novae is approximately Gaussian (with the right tail truncated at $1.4 M_\odot$). The best fit Gaussian is characterized by $\langle M_{WD} \rangle = 1.16 \pm 0.14 M_\odot$, which is virtually identical to the mean and RMS deviation (1.15, 0.14) derived directly from the individual masses. Both the mean and dispersion of the observed WD mass distribution are remarkably similar to those found by Shara et al. (2018) for Galactic novae, with the average observed WD mass of M31 novae being just $\sim 0.03 M_\odot$ larger than the Galactic average. However, the mean WD mass for our M31 nova sample is $\sim 0.15 M_\odot$ higher than that recently found by Schaefer (2025) in his comprehensive study of more than 300 Galactic novae.

(2) As expected, the estimated WD masses for known RNe cluster toward the high mass end of the distribution. The mean observed WD mass for RNe was found to be $\langle M_{WD}(RN) \rangle = 1.33 \pm 0.08 M_\odot$, while the mean intrinsic WD mass was found to be $\langle M_{WD,int}(RN) \rangle = 1.27 \pm 0.10 M_\odot$.

(3) The observed accretion rate distribution is highly skewed towards lower accretion rates and is characterized by $\langle \log \dot{M} \rangle = -9.3 \pm 1.4$, corresponding to an accretion rate of $5 \times 10^{-10} M_\odot \text{ yr}^{-1}$. An excess of systems with estimated accretion rates near $10^{-7} M_\odot \text{ yr}^{-1}$ is seen, and is possibly an artefact caused by the truncation of the model grid for $\log \dot{M} > -7$. It is also possible that the spike near $\log \dot{M} = -7$ is real, reflecting a subpopulation of novae with evolved secondary stars producing higher accretion rates.

(4) As noted by Shara et al. (2018) in their study of Galactic novae, the observed distributions for M_{WD} and $\log \dot{M}$ will be biased toward systems with short recurrence times. The intrinsic (unbiased) WD mass and $\log \dot{M}$ distributions, which were estimated by weighting the observed distributions by the recurrence times of the novae, are characterized by means of $\langle M_{WD} \rangle = 1.07 M_\odot$ and $\langle \log \dot{M} \rangle = -10.7$. The mean of the intrinsic WD mass distribution is $\sim 0.1 M_\odot$.

² We have transformed our values of M_R to M_V using the expected $V - R$ color of novae near peak brightness given in Craig et al. (2025).

³ Errors reported are standard errors of the mean

lower than the observed mean, which is similar to the $0.07 M_{\odot}$ difference between the observed and intrinsic means found by [Shara et al. \(2018\)](#) in their study of Galactic novae. The estimated mean intrinsic accretion rate for M31 novae appears to be remarkably low, of order $10^{-11} M_{\odot} \text{ yr}^{-1}$, which is about an order of magnitude lower than that estimated by [Shara et al. \(2018\)](#) for Galactic novae. The source of the discrepancy is unclear, but if the eruption amplitude is used as a model input, inferred accretion rates can be overestimated in low-outburst-amplitude systems with evolved (luminous) secondary stars.

(5) The low accretion rates and long recurrence times inferred for both our M31 sample and for the Galactic novae studied by [Shara et al. \(2018\)](#) are likely the result of novae spending most of their inter-eruption time in hibernation (e.g., see [Shara et al. 1986](#)).

(6) The isophotal radius of each M31 nova was computed and used to explore the potential variation of nova properties with distance from the center of M31. No systematic variation with isophotal radius was found for WD masses or t_2 times for the novae in our sample. However, there was weak evidence suggesting that the peak luminosity, accretion rate, recurrence time, and possibly the maximum ejection velocity might vary with distance from the center of M31. We do not consider this evidence to be compelling given uncertainties in distinguishing bulge and disk populations from a alone, and because of the unknown effects of extinction across M31. This skepticism is reinforced by considering the cumulative distributions of “fast” ($t_2 \leq 25$ d) and “slow” ($t_2 > 25$ d) novae, and of Fe II and He/N novae in cases where the spectroscopic type is known, which show no significant variation with isophotal radius. Overall, we find no compelling evidence that the properties of novae are sensitive to stellar population (bulge vs. disk) in M31.

(7) The M31 and Galactic nova populations appear to be qualitatively similar in terms of the global nova rate, but differ slightly in terms of average light curve properties (M_V and t_2 time distributions). In particular, the Galactic novae are on average brighter ($> 3\sigma$ significance) and faster (1.9σ significance) than their M31 counterparts. This matches expectations for novae arising in a galaxy with a slightly later Hubble type and more recent star formation.

The principal focus of our study has been to compare the fundamental properties of M31 novae – particularly the WD mass and accretion rate distributions – with their Galactic counterparts. The mean mass accretion rate for M31 novae is surprisingly low, of order $10^{-10} M_{\odot} \text{ yr}^{-1}$ and $10^{-11} M_{\odot} \text{ yr}^{-1}$ for the apparent and intrinsic distributions, respectively. Both of these numbers are approximately an order of magnitude lower than those found for Galactic novae. On the other hand, the M31 WD mass distribution is remarkably similar to that found by [Shara et al. \(2018\)](#) for a sample of 82 Galactic novae, but it is about 10 to 15% higher than that recently found by [Schaefer \(2025\)](#) in his comprehensive study of Galactic novae. In the latter case, the key difference being the dearth of M31 novae with $M_{\text{WD}} < 1 M_{\odot}$, or 11%, compared with $\sim 50\%$ in the [Schaefer \(2025\)](#) sample. A more reliable comparison of the M31 and Galactic nova populations will require more accurate observations (more complete light curves) coupled with more detailed nova models.

We thank the anonymous referee for constructive suggestions that helped improve our paper. K.H. was supported by the RVO:67985815.

Table 1. Nova Model Grid^a

$\log \dot{M}$ ($M_{\odot} \text{ yr}^{-1}$)	M_{WD} (M_{\odot})	L_4 ($10^4 L_{\odot}$)	t_{ml} (days)	V_{max} (km s $^{-1}$)	P_{rec} (yr)
-7	0.65	1.48	2.45E+02
-7	1.00	3.45	210	265	8.96E+01
-7	1.25	4.84	65.1	414	1.92E+01
-7	1.40	6.03	4.13	1410	7.71E-01
-8	0.65	1.52	1170	156	1.01E+04
-8	1.00	3.26	127	351	2.06E+03
-8	1.25	6.38	20.2	1110	3.67E+02
-8	1.40	9.27	1.57	3060	1.64E+01
-9	0.65	4.76	264	2590	1.61E+05
-9	1.00	3.88	93.5	525	4.66E+04
-9	1.25	6.67	9.56	1480	9.27E+03
-9	1.40	9.23	1.39	2850	4.12E+02
-10	0.65	13.7	117	4210	2.55E+06
-10	1.00	11.3	33.6	1920	8.40E+05
-10	1.25	7.14	24.3	2230	1.91E+05
-10	1.40	10.1	0.678	5270	5.90E+03
-11	0.65	5.98	27.6	1300	2.58E+07
-11	1.00	6.08	35.4	1250	8.72E+06
-11	1.25	69.4	9.31	4240	2.97E+06
-11	1.40	37.5	2.95	4460	2.59E+05
-12	0.65	20.7	110	682	3.94E+08
-12	1.00	9.80	55.3	1230	9.28E+07
-12	1.25	184	58.6	9680	3.22E+07
-12	1.40

^a From Yaron et al. (2005), Table 3, $T_{\text{WD}} = 10 \times 10^6$ K.

Table 2. Linear Lightcurve Nova Parameters

Nova (M31N)	Quality	L_4 ($10^4 L_{\odot}$)	t_2 (days)	$\log \dot{M}$ ($M_{\odot} \text{ yr}^{-1}$)	M_{WD} (M_{\odot})	V_{max} (km s $^{-1}$)	$\log P_{\text{rec}}$ (yr)	Type
2002-08a	Silver	6.92 ± 1.10	44.4 ± 10.3	-10.00 ± 0.50	1.00 ± 0.11	1256 ± 495	6.01 ± 0.68	FeII:
2004-08b	Silver	5.50 ± 1.04	47.4 ± 18.0	-9.53 ± 0.87	1.01 ± 0.13	1091 ± 567	5.41 ± 1.15	FeII
2004-09a	Silver	4.57 ± 0.72	27.4 ± 10.1	-8.35 ± 0.76	1.16 ± 0.07	895 ± 527	3.31 ± 1.07	FeII
2004-11a	Silver	11.48 ± 2.18	19.0 ± 12.0	-10.31 ± 0.37	1.14 ± 0.06	1995 ± 705	5.89 ± 0.52	FeII
2004-11b	Silver	10.47 ± 1.66	37.7 ± 9.7	-10.56 ± 0.36	1.03 ± 0.09	1531 ± 541	6.58 ± 0.50	FeIIB
2005-01a	Silver	43.65 ± 5.97	18.7 ± 2.4	-11.62 ± 0.21	1.26 ± 0.04	3673 ± 1461	6.88 ± 0.33	FeII
2005-07a	Bronze	5.01 ± 0.95	9.4 ± 6.1	-7.20 ± 0.96	1.33 ± 0.07	785 ± 641	0.75 ± 0.95	FeII
2006-06a	Gold	4.17 ± 0.66	37.6 ± 2.8	-8.21 ± 0.83	1.14 ± 0.07	760 ± 490	3.22 ± 1.18	FeII
2006-09c	Gold	7.24 ± 1.15	14.9 ± 2.7	-9.36 ± 0.46	1.18 ± 0.03	1633 ± 576	4.56 ± 0.61	FeII
2006-12a	Gold	5.50 ± 1.04	33.1 ± 4.6	-9.24 ± 0.93	1.08 ± 0.07	1140 ± 607	4.80 ± 1.22	FeII
2007-02b	Gold	9.91 ± 1.57	31.7 ± 5.7	-10.38 ± 0.29	1.06 ± 0.03	1589 ± 485	6.27 ± 0.37	FeII:
2007-07e	Silver	3.16 ± 0.84	43.5 ± 5.8	-7.00 :	1.23 ± 0.13	414 ± 464	1.04 ± 1.16	FeII
2007-11b	Bronze	2.19 ± 0.41	47.4 ± 4.4	-7.00 :	1.20 ± 0.01	363 ± 127	1.22 ± 0.12	He/Nn
2007-12b	Bronze	7.24 ± 1.15	6.5 ± 0.5	-8.80 ± 0.92	1.28 ± 0.04	1897 ± 1107	3.31 ± 1.26	He/N
2008-05c	Silver	6.03 ± 0.95	29.4 ± 5.1	-9.39 ± 0.61	1.09 ± 0.05	1247 ± 513	4.96 ± 0.80	FeII
2008-06b	Silver	18.20 ± 2.88	23.8 ± 6.9	-10.97 ± 0.21	1.14 ± 0.03	2239 ± 625	6.66 ± 0.29	He/N

Table 2 continued on next page

Table 2 (*continued*)

Nova (M31N)	L_4 ($10^4 L_\odot$)	t_2 (days)	$\log \dot{M}$ ($M_\odot \text{ yr}^{-1}$)	M_{WD} (M_\odot)	V_{max} (km s^{-1})	$\log P_{\text{rec}}$ (yr)	Type	
2008-07b	Silver	2.00 ± 0.32	23.5 ± 7.7	$-7.00 :$	1.21 ± 0.00	382 ± 134	1.15 ± 0.12	FeII
2008-08a	Silver	9.55 ± 1.51	17.1 ± 4.4	-9.98 ± 0.31	1.15 ± 0.03	1888 ± 573	5.44 ± 0.41	FeII
2008-10b	Bronze	2.88 ± 0.55	54.1 ± 9.3	-7.01 ± 1.10	1.21 ± 0.12	386 ± 366	1.16 ± 1.02	FeII
2008-11a	Bronze	11.48 ± 1.82	4.8 ± 1.5	-9.61 ± 0.32	1.30 ± 0.02	3048 ± 910	4.26 ± 0.44	He/N
2009-08d	Bronze	6.03 ± 0.95	33.9 ± 13.3	-9.50 ± 0.66	1.06 ± 0.07	1219 ± 528	5.19 ± 0.87	FeII
2009-08e	Silver	3.16 ± 0.50	118.9 ± 30.3	-7.64 ± 1.31	1.08 ± 0.22	422 ± 498	2.69 ± 1.58	FeII
2009-09a	Bronze	4.57 ± 0.87	124.2 ± 43.1	-9.70 ± 0.87	0.68 ± 0.21	1130 ± 466	6.00 ± 1.03	FeII
2009-10c	Gold	12.59 ± 2.38	33.6 ± 6.7	-10.73 ± 0.26	1.06 ± 0.04	1698 ± 497	6.68 ± 0.34	FeII
2009-11a	Gold	4.17 ± 0.66	23.9 ± 2.1	-7.34 ± 1.10	1.25 ± 0.09	605 ± 547	1.43 ± 1.14	FeII
2009-11c	Gold	7.05 ± 1.12	30.1 ± 7.7	-9.77 ± 0.41	1.07 ± 0.04	1377 ± 477	5.50 ± 0.53	FeII
2009-11d	Gold	5.70 ± 0.90	23.9 ± 2.2	-9.10 ± 0.92	1.13 ± 0.06	1233 ± 676	4.43 ± 1.22	FeII
2009-11e	Bronze	7.24 ± 1.15	38.8 ± 15.1	-9.99 ± 0.47	1.02 ± 0.09	1318 ± 514	5.92 ± 0.64	FeII
2010-05a	Gold	7.24 ± 1.15	37.5 ± 6.8	-9.97 ± 0.38	1.03 ± 0.04	1327 ± 443	5.88 ± 0.49	FeII
2010-09b	Gold	2.40 ± 0.45	18.0 ± 2.2	$-7.00 :$	1.28 ± 0.02	512 ± 188	0.77 ± 0.18	FeII
2010-10c	Gold	2.51 ± 0.40	30.1 ± 3.9	$-7.00 :$	1.25 ± 0.02	443 ± 162	0.95 ± 0.19	FeII
2011-01a	Gold	49.20 ± 6.73	8.4 ± 4.4	-11.44 ± 0.27	1.34 ± 0.03	5636 ± 2424	6.22 ± 0.39	FeII
2011-02a	Bronze	6.03 ± 0.95	24.9 ± 6.5	-9.27 ± 0.79	1.12 ± 0.06	1279 ± 622	4.70 ± 1.04	...
2011-02b	Bronze	3.80 ± 0.85	14.0 ± 2.6	$-7.00 :$	1.32 ± 0.06	614 ± 418	0.54 ± 0.71	...
2011-02c	Bronze	7.94 ± 1.50	11.3 ± 2.1	-9.39 ± 0.45	1.21 ± 0.03	1866 ± 633	4.45 ± 0.60	...
2011-02d	Gold	7.94 ± 1.26	23.3 ± 5.8	-9.83 ± 0.36	1.11 ± 0.03	1563 ± 515	5.43 ± 0.47	...
2011-06b	Gold	1.85 ± 0.29	42.1 ± 4.7	$-7.00 :$	1.21 ± 0.06	383 ± 197	1.15 ± 0.51	...
2011-06d	Gold	7.94 ± 1.26	17.2 ± 2.2	-9.65 ± 0.36	1.15 ± 0.02	1687 ± 539	5.03 ± 0.47	FeII
2011-07a	Silver	12.02 ± 1.81	22.6 ± 5.4	-10.46 ± 0.25	1.12 ± 0.03	1923 ± 556	6.15 ± 0.33	FeII
2011-07b	Gold	4.57 ± 0.72	23.4 ± 2.6	-8.11 ± 0.77	1.19 ± 0.06	861 ± 532	2.83 ± 1.10	FeII
2011-08b	Gold	8.55 ± 1.17	35.2 ± 9.4	-10.21 ± 0.32	1.04 ± 0.04	1449 ± 466	6.14 ± 0.42	FeII
2011-12b	Bronze	2.40 ± 0.45	67.5 ± 12.5	$-7.00 :$	1.20 ± 0.07	361 ± 193	1.23 ± 0.55	FeII
2012-01a	Silver	5.01 ± 0.79	34.8 ± 8.7	-9.00 ± 0.91	1.09 ± 0.08	1038 ± 584	4.47 ± 1.21	FeII
2012-02c	Gold	7.59 ± 1.20	28.6 ± 5.3	-9.88 ± 0.37	1.08 ± 0.03	1452 ± 482	5.61 ± 0.48	...
2012-03b	Bronze	5.01 ± 0.95	43.5 ± 22.7	-9.19 ± 0.98	1.04 ± 0.12	1021 ± 610	4.87 ± 1.31	...
2012-03c	Bronze	11.48 ± 1.82	39.7 ± 8.1	-10.71 ± 0.38	1.03 ± 0.12	1552 ± 626	6.77 ± 0.56	...
2012-05c	Gold	5.50 ± 0.87	21.7 ± 4.0	-8.90 ± 0.89	1.15 ± 0.06	1194 ± 677	4.08 ± 1.20	...
2012-05d	Gold	2.00 ± 0.53	33.0 ± 5.6	$-7.00 :$	1.25 ± 0.07	440 ± 252	0.97 ± 0.59	...
2012-06a	Silver	9.82 ± 1.41	33.2 ± 12.1	-10.39 ± 0.31	1.05 ± 0.05	1560 ± 499	6.31 ± 0.41	FeII
2012-06f	Bronze	1.66 ± 0.26	34.4 ± 12.7	$-7.00 :$	1.16 ± 0.00	318 ± 113	1.41 ± 0.11	FeII
2012-06g	Gold	7.45 ± 1.12	20.0 ± 4.6	-9.62 ± 0.39	1.13 ± 0.03	1567 ± 526	5.07 ± 0.51	He/N
2012-07a	Bronze	3.16 ± 0.60	58.0 ± 21.9	-7.29 ± 1.17	1.18 ± 0.13	434 ± 432	1.75 ± 1.21	FeII
2012-07b	Silver	8.71 ± 1.25	29.5 ± 4.0	-10.14 ± 0.31	1.07 ± 0.03	1538 ± 483	5.95 ± 0.40	...
2013-02b	Bronze	3.47 ± 0.55	14.9 ± 1.1	$-7.00 :$	1.31 ± 0.04	596 ± 268	0.57 ± 0.38	...
2013-03b	Bronze	9.55 ± 1.51	43.6 ± 17.6	-10.52 ± 0.51	1.00 ± 0.17	1419 ± 685	6.63 ± 0.75	...
2013-06a	Bronze	6.61 ± 1.75	12.3 ± 4.6	-9.01 ± 0.96	1.21 ± 0.06	1563 ± 908	3.96 ± 1.29	...
2013-08a	Gold	4.17 ± 0.79	8.7 ± 1.4	-7.01 ± 0.64	1.35 ± 0.05	733 ± 435	0.34 ± 0.58	He/N:
2013-10g	Bronze	6.85 ± 0.99	47.1 ± 8.2	-10.02 ± 0.51	0.99 ± 0.12	1233 ± 491	6.07 ± 0.69	FeII
2014-01c	Silver	6.61 ± 1.25	34.2 ± 4.6	-9.72 ± 0.45	1.05 ± 0.04	1291 ± 456	5.50 ± 0.58	...
2014-06a	Gold	10.47 ± 1.98	21.1 ± 4.4	-10.23 ± 0.30	1.13 ± 0.03	1849 ± 551	5.86 ± 0.39	...
2014-07a	Gold	4.57 ± 0.72	47.3 ± 5.8	-8.96 ± 0.89	1.05 ± 0.08	925 ± 516	4.55 ± 1.19	FeII
2014-09a	Gold	12.59 ± 2.38	16.7 ± 2.6	-10.37 ± 0.26	1.16 ± 0.02	2178 ± 599	5.87 ± 0.34	FeII
2015-05b	Silver	7.24 ± 1.15	21.0 ± 3.7	-9.59 ± 0.40	1.13 ± 0.03	1517 ± 513	5.06 ± 0.52	FeII
2015-06a	Bronze	52.00 ± 7.11	6.5 ± 0.3	-11.40 ± 0.27	1.37 ± 0.02	6546 ± 2817	6.02 ± 0.36	FeII
2015-07d	Silver	30.20 ± 4.34	6.6 ± 0.7	-10.94 ± 0.23	1.32 ± 0.02	4819 ± 1506	5.77 ± 0.32	FeII
2015-08a	Silver	5.70 ± 0.90	41.5 ± 7.1	-9.51 ± 0.58	1.03 ± 0.06	1135 ± 450	5.31 ± 0.75	FeII
2015-09a	Bronze	45.29 ± 6.19	12.2 ± 0.8	-11.50 ± 0.27	1.30 ± 0.04	4560 ± 1891	6.51 ± 0.40	...
2015-10a	Silver	35.97 ± 5.43	8.1 ± 0.8	-11.17 ± 0.26	1.32 ± 0.03	4875 ± 1711	6.05 ± 0.36	FeIIB

Table 2 continued on next page

Table 2 (*continued*)

Nova		L_4	t_2	$\log \dot{M}$	M_{WD}	V_{max}	$\log P_{\text{rec}}$	
(M31N)	Quality	($10^4 L_\odot$)	(days)	($M_\odot \text{ yr}^{-1}$)	(M_\odot)	(km s^{-1})	(yr)	Type
2015-11b	Bronze	0.95 ± 0.18	32.2 ± 5.5	-7.38 ± 0.23	1.12 ± 0.03	390 ± 142	2.13 ± 0.36	...
2016-03b	Bronze	5.70 ± 0.90	41.5 ± 7.1	-9.51 ± 0.58	1.03 ± 0.06	1135 ± 450	5.31 ± 0.75	...
2016-10b	Silver	9.46 ± 1.43	28.6 ± 5.5	-10.25 ± 0.30	1.08 ± 0.03	1607 ± 494	6.07 ± 0.38	FeII
2016-10c	Silver	10.47 ± 2.33	26.3 ± 10.9	-10.35 ± 0.34	1.10 ± 0.05	1722 ± 551	6.12 ± 0.45	...
2016-12b	Bronze	5.01 ± 0.95	41.4 ± 16.0	-9.15 ± 0.95	1.05 ± 0.09	1026 ± 577	4.78 ± 1.26	...
2016-12d	Silver	15.85 ± 2.28	30.8 ± 7.0	-10.94 ± 0.21	1.10 ± 0.04	1905 ± 544	6.81 ± 0.28	FeIIB
2017-01a	Bronze	9.55 ± 5.43	10.6 ± 2.0	-9.71 ± 1.30	1.21 ± 0.05	2153 ± 1147	4.84 ± 1.66	...
2017-01c	Silver	19.59 ± 2.82	18.7 ± 7.3	-10.93 ± 0.21	1.18 ± 0.04	2541 ± 723	6.46 ± 0.30	FeII
2017-02a	Bronze	5.50 ± 0.87	6.7 ± 0.7	-7.15 ± 0.96	1.36 ± 0.06	879 ± 685	0.48 ± 0.87	...
2017-03a	Silver	7.24 ± 1.37	17.5 ± 3.3	-9.47 ± 0.45	1.15 ± 0.03	1581 ± 553	4.80 ± 0.59	FeII
2017-03b	Silver	6.03 ± 1.86	21.1 ± 2.3	-9.15 ± 0.99	1.14 ± 0.06	1318 ± 740	4.44 ± 1.31	...
2017-04b	Gold	13.80 ± 2.18	25.9 ± 7.0	-10.70 ± 0.24	1.11 ± 0.03	1936 ± 555	6.47 ± 0.32	...
2017-06a	Gold	11.48 ± 1.82	26.6 ± 6.1	-10.48 ± 0.26	1.10 ± 0.03	1782 ± 525	6.27 ± 0.34	...
2017-08a	Gold	4.79 ± 0.76	20.6 ± 3.7	-8.24 ± 0.74	1.20 ± 0.05	951 ± 552	2.99 ± 1.05	...
2017-10b	Silver	5.50 ± 1.04	33.6 ± 11.6	-9.25 ± 0.93	1.08 ± 0.08	1135 ± 614	4.83 ± 1.22	...
2019-03a	Gold	49.66 ± 6.79	10.2 ± 3.0	-11.51 ± 0.24	1.33 ± 0.03	5188 ± 2223	6.39 ± 0.36	FeII

Table 3. Break Lightcurve Nova Parameters

Nova		L_4	t_2	$\log \dot{M}$	M_{WD}	V_{max}	$\log P_{\text{rec}}$	
(M31N)	Quality	($10^4 L_\odot$)	(days)	($M_\odot \text{ yr}^{-1}$)	(M_\odot)	(km s^{-1})	(yr)	Type
2006-11a	Gold	18.20 ± 2.88	21.8 ± 4.5	-10.93 ± 0.20	1.16 ± 0.03	2317 ± 628	6.57 ± 0.27	FeII
2009-10b	Silver	22.70 ± 3.10	6.8 ± 2.3	-10.67 ± 0.21	1.30 ± 0.03	4102 ± 1166	5.58 ± 0.30	FeII
2010-01a	Gold	19.23 ± 2.63	14.3 ± 3.1	-10.80 ± 0.19	1.21 ± 0.02	2812 ± 735	6.18 ± 0.26	FeII
2010-01b	Gold	8.71 ± 1.65	23.7 ± 9.7	-10.01 ± 0.38	1.11 ± 0.05	1633 ± 548	5.67 ± 0.50	...
2010-01c	Bronze	8.32 ± 1.26	7.6 ± 2.6	-9.24 ± 0.63	1.25 ± 0.04	2109 ± 893	4.03 ± 0.85	...
2010-02a	Gold	27.80 ± 4.19	5.1 ± 2.3	-10.76 ± 0.25	1.34 ± 0.03	5129 ± 1706	5.46 ± 0.36	...
2010-03a	Silver	7.24 ± 1.61	63.7 ± 11.6	-10.37 ± 0.43	0.89 ± 0.12	1205 ± 377	6.68 ± 0.54	...
2010-06a	Gold	7.59 ± 1.20	49.8 ± 3.9	-10.25 ± 0.51	0.97 ± 0.14	1271 ± 505	6.39 ± 0.69	FeII
2010-06c	Gold	4.79 ± 0.76	23.0 ± 6.8	-8.38 ± 0.75	1.18 ± 0.06	966 ± 553	3.28 ± 1.06	...
2010-07a	Gold	16.14 ± 2.32	17.3 ± 6.6	-10.69 ± 0.23	1.18 ± 0.03	2415 ± 677	6.20 ± 0.32	FeII
2010-10a	Gold	6.37 ± 1.01	10.4 ± 2.9	-8.76 ± 0.86	1.23 ± 0.05	1524 ± 869	3.49 ± 1.18	FeII
2010-10d	Gold	7.24 ± 1.15	22.9 ± 3.9	-9.65 ± 0.40	1.12 ± 0.03	1489 ± 502	5.19 ± 0.52	FeII
2010-12c	Gold	11.48 ± 1.82	6.9 ± 2.2	-9.80 ± 0.30	1.26 ± 0.02	2754 ± 793	4.70 ± 0.41	...
2011-01b	Gold	13.06 ± 1.79	3.4 ± 0.9	-9.65 ± 0.29	1.33 ± 0.02	3698 ± 1088	4.11 ± 0.40	...
2011-06a	Gold	3.47 ± 0.55	35.8 ± 9.5	$-7.00 :$	1.25 ± 0.12	440 ± 473	0.97 ± 1.12	FeII
2011-08a	Gold	3.98 ± 0.63	27.7 ± 3.0	-7.32 ± 1.13	1.24 ± 0.09	568 ± 526	1.47 ± 1.15	FeII
2011-09a	Gold	11.91 ± 1.63	19.5 ± 7.4	-10.37 ± 0.26	1.14 ± 0.04	2014 ± 599	5.96 ± 0.36	FeII
2011-09b	Gold	9.12 ± 1.31	9.9 ± 2.9	-9.59 ± 0.34	1.22 ± 0.03	2128 ± 658	4.65 ± 0.46	FeII
2011-10a	Bronze	9.04 ± 1.24	43.9 ± 9.4	-10.44 ± 0.49	1.00 ± 0.15	1393 ± 598	6.54 ± 0.69	FeII
2011-10d	Gold	8.87 ± 1.27	29.0 ± 10.4	-10.16 ± 0.33	1.08 ± 0.05	1556 ± 508	5.97 ± 0.44	FeIIB
2011-11c	Gold	10.28 ± 1.55	22.7 ± 3.6	-10.25 ± 0.27	1.12 ± 0.03	1795 ± 531	5.93 ± 0.35	FeII
2011-11e	Silver	17.06 ± 2.45	39.5 ± 9.5	-11.15 ± 0.28	1.06 ± 0.13	1770 ± 830	7.16 ± 0.53	FeII
2011-12a	Gold	5.70 ± 0.86	30.8 ± 14.3	-9.29 ± 0.88	1.09 ± 0.09	1189 ± 634	4.84 ± 1.17	FeII
2012-02b	Gold	34.67 ± 4.51	4.1 ± 1.5	-10.90 ± 0.28	1.37 ± 0.02	6353 ± 2262	5.41 ± 0.37	...
2012-05a	Gold	32.81 ± 4.72	17.4 ± 5.2	-11.37 ± 0.22	1.24 ± 0.03	3311 ± 1082	6.71 ± 0.32	...
2012-06e	Gold	2.88 ± 0.55	16.1 ± 12.1	$-7.00 :$	1.29 ± 0.03	535 ± 211	0.71 ± 0.25	FeII

Table 3 continued on next page

Table 3 (*continued*)

Nova (M31N)	L_4 ($10^4 L_\odot$)	t_2 (days)	$\log \dot{M}$ ($M_\odot \text{ yr}^{-1}$)	M_{WD} (M_\odot)	V_{max} (km s^{-1})	$\log P_{\text{rec}}$ (yr)	Type	
Quality								
2012-07c	Gold	7.18 ± 1.03	27.4 ± 7.2	-9.74 ± 0.39	1.09 ± 0.04	1419 ± 487	5.41 ± 0.51	FeII
2012-09b	Gold	27.54 ± 3.77	3.2 ± 0.4	-10.58 ± 0.25	1.37 ± 0.02	6109 ± 1979	5.02 ± 0.34	FeIIB
2013-04a	Gold	13.80 ± 2.18	9.4 ± 5.1	-10.22 ± 0.30	1.24 ± 0.04	2786 ± 875	5.36 ± 0.43	...
2013-06b	Silver	14.72 ± 2.22	21.9 ± 7.0	-10.70 ± 0.23	1.14 ± 0.03	2113 ± 598	6.37 ± 0.31	FeII
2013-08b	Silver	12.59 ± 2.38	23.4 ± 9.0	-10.54 ± 0.28	1.12 ± 0.04	1932 ± 580	6.26 ± 0.38	...
2013-09a	Silver	3.47 ± 0.55	29.9 ± 8.8	$-7.00 :$	1.26 ± 0.10	467 ± 443	0.88 ± 1.00	...
2013-09c	Gold	12.13 ± 1.74	16.8 ± 3.0	-10.32 ± 0.24	1.16 ± 0.02	2138 ± 594	5.82 ± 0.32	...
2013-09d	Bronze	6.85 ± 0.99	62.7 ± 26.0	-10.24 ± 0.43	0.90 ± 0.13	1180 ± 386	6.51 ± 0.56	FeII
2013-10a	Gold	12.59 ± 1.90	18.3 ± 4.3	-10.41 ± 0.24	1.15 ± 0.03	2113 ± 592	5.96 ± 0.32	FeII
2013-10e	Bronze	11.48 ± 1.82	9.6 ± 5.5	-9.96 ± 0.35	1.23 ± 0.05	2483 ± 839	5.08 ± 0.50	...
2013-10h	Bronze	22.70 ± 3.10	14.5 ± 3.7	-10.97 ± 0.19	1.22 ± 0.03	3020 ± 813	6.32 ± 0.27	FeII
2013-12b	Gold	22.49 ± 3.23	7.0 ± 2.8	-10.67 ± 0.22	1.29 ± 0.03	4018 ± 1175	5.60 ± 0.32	FeIIB
2014-01a	Gold	15.85 ± 2.28	11.6 ± 2.2	-10.49 ± 0.21	1.22 ± 0.02	2780 ± 714	5.76 ± 0.28	FeII
2014-06b	Gold	7.94 ± 1.26	27.6 ± 5.2	-9.94 ± 0.35	1.08 ± 0.03	1500 ± 489	5.67 ± 0.45	He/N:
2014-12a	Gold	49.66 ± 6.79	10.8 ± 3.9	-11.53 ± 0.23	1.32 ± 0.04	5070 ± 2206	6.43 ± 0.36	...
2015-09c	Gold	90.37 ± 12.99	4.7 ± 0.8	-11.68 ± 0.14	1.40 ± 0.01	8017 ± 4275	6.13 ± 0.23	FeII
2015-09d	Silver	16.60 ± 2.63	13.6 ± 10.2	-10.61 ± 0.36	1.21 ± 0.07	2679 ± 1043	5.97 ± 0.55	...
2016-05a	Silver	5.50 ± 0.87	24.3 ± 4.5	-9.00 ± 0.92	1.13 ± 0.07	1186 ± 668	4.29 ± 1.23	FeII
2016-08b	Gold	7.24 ± 1.15	42.6 ± 4.3	-10.05 ± 0.44	1.00 ± 0.08	1288 ± 467	6.05 ± 0.58	...
2016-08d	Gold	36.98 ± 5.06	11.8 ± 1.1	-11.33 ± 0.25	1.29 ± 0.03	4178 ± 1457	6.41 ± 0.35	FeII
2016-11a	Gold	21.68 ± 3.12	8.6 ± 2.2	-10.71 ± 0.20	1.27 ± 0.02	3648 ± 978	5.76 ± 0.28	FeIIB
2016-11b	Gold	17.70 ± 2.42	12.6 ± 1.8	-10.65 ± 0.19	1.22 ± 0.02	2838 ± 721	5.96 ± 0.26	...
2016-12a	Silver	6.03 ± 0.91	41.4 ± 9.0	-9.65 ± 0.48	1.02 ± 0.06	1180 ± 437	5.51 ± 0.63	...
2016-12c	Gold	9.29 ± 1.40	22.3 ± 6.0	-10.08 ± 0.31	1.12 ± 0.03	1718 ± 536	5.72 ± 0.41	...
2017-01d	Gold	13.80 ± 2.18	19.1 ± 9.7	-10.55 ± 0.28	1.15 ± 0.05	2163 ± 669	6.14 ± 0.39	...
2017-11e	Silver	12.59 ± 1.99	4.7 ± 1.2	-9.75 ± 0.29	1.30 ± 0.02	3273 ± 924	4.42 ± 0.39	He/N

Table 4. Jitter Lightcurve Nova Parameters

Nova (M31N)	Quality	L_4 ($10^4 L_\odot$)	t_2 (days)	$\log \dot{M}$ ($M_\odot \text{ yr}^{-1}$)	M_{WD} (M_\odot)	V_{max} (km s^{-1})	$\log P_{\text{rec}}$ (yr)	Type
2006-10a	Bronze	3.16 ± 0.50	67.6 ± 34.4	-7.48 ± 1.17	1.14 ± 0.16	453 ± 477	2.18 ± 1.37	FeII
2008-07a	Bronze	1.51 ± 0.40	482.5 ± 103.5	-7.01 ± 0.44	0.96 ± 0.14	201 ± 106	2.19 ± 0.51	FeII
2009-08a	Bronze	3.47 ± 0.55	92.0 ± 36.8	-8.27 ± 0.95	1.03 ± 0.17	594 ± 457	3.72 ± 1.39	FeII
2010-06b	Bronze	3.98 ± 0.63	69.7 ± 62.6	-8.77 ± 0.91	1.01 ± 0.18	773 ± 528	4.43 ± 1.30	FeII
2010-06d	Bronze	3.87 ± 0.61	95.0 ± 91.5	-9.00 ± 0.97	0.93 ± 0.19	776 ± 459	4.93 ± 1.31	FeII
2010-10b	Bronze	4.17 ± 0.66	211.4 ± 151.1	-9.44 ± 0.95	0.65 ± 0.27	1079 ± 514	5.67 ± 1.14	FeII
2010-11a	Bronze	2.63 ± 0.42	44.9 ± 25.6	$-7.00 :$	1.22 ± 0.10	397 ± 272	1.10 ± 0.74	He/Nn
2011-05a	Bronze	7.24 ± 1.61	74.3 ± 25.2	-10.61 ± 0.46	0.75 ± 0.13	1282 ± 384	7.06 ± 0.53	...
2011-11a	Silver	3.63 ± 0.57	33.2 ± 8.9	-7.12 ± 1.21	1.24 ± 0.11	481 ± 491	1.16 ± 1.13	FeII
2012-05b	Bronze	2.40 ± 0.45	60.2 ± 28.0	$-7.00 :$	1.20 ± 0.09	363 ± 213	1.22 ± 0.62	...
2013-10b	Bronze	5.01 ± 0.95	27.1 ± 7.5	-8.77 ± 0.84	1.13 ± 0.07	1050 ± 593	3.99 ± 1.14	...
2013-12a	Bronze	2.63 ± 0.42	166.8 ± 58.9	-7.67 ± 0.97	1.03 ± 0.19	390 ± 337	2.90 ± 1.29	He/Nn
2014-05a	Bronze	4.57 ± 0.87	54.4 ± 23.1	-9.09 ± 0.96	1.02 ± 0.14	920 ± 563	4.82 ± 1.30	...
2014-10a	Bronze	3.84 ± 0.55	91.1 ± 55.0	-8.91 ± 0.85	0.95 ± 0.15	757 ± 416	4.77 ± 1.15	FeII
2014-11a	Bronze	3.80 ± 0.72	110.2 ± 32.1	-9.09 ± 0.85	0.89 ± 0.14	782 ± 383	5.13 ± 1.10	...
2014-12b	Bronze	4.57 ± 0.72	38.1 ± 32.1	-8.74 ± 0.91	1.10 ± 0.13	923 ± 642	4.11 ± 1.30	...
2015-03a	Bronze	2.88 ± 0.46	127.1 ± 72.0	-7.72 ± 1.01	1.05 ± 0.18	426 ± 385	2.89 ± 1.36	...
2015-04a	Bronze	3.47 ± 0.55	116.5 ± 49.0	-8.67 ± 0.80	0.94 ± 0.14	659 ± 361	4.49 ± 1.09	...
2015-05c	Bronze	2.63 ± 0.50	82.2 ± 24.2	$-7.00 :$	1.18 ± 0.14	336 ± 345	1.33 ± 1.09	...
2015-06b	Bronze	5.01 ± 0.79	87.2 ± 72.6	-9.84 ± 1.11	0.83 ± 0.23	1033 ± 508	6.13 ± 1.35	...
2015-10b	Bronze	5.45 ± 0.82	100.3 ± 75.8	-10.12 ± 0.93	0.72 ± 0.25	1194 ± 431	6.50 ± 1.09	FeII
2015-11c	Bronze	5.01 ± 0.79	51.8 ± 18.2	-9.34 ± 0.94	1.01 ± 0.14	1007 ± 566	5.17 ± 1.25	FeII
2016-03d	Bronze	4.17 ± 0.79	80.1 ± 24.5	-9.13 ± 0.90	0.95 ± 0.15	839 ± 450	5.06 ± 1.19	...
2016-08e	Silver	6.61 ± 1.05	60.6 ± 16.7	-10.14 ± 0.45	0.92 ± 0.13	1167 ± 403	6.36 ± 0.59	FeII
2016-09a	Bronze	4.57 ± 0.72	57.0 ± 35.1	-9.13 ± 0.95	1.01 ± 0.16	918 ± 563	4.91 ± 1.29	FeII
2016-09b	Silver	5.50 ± 0.87	43.9 ± 17.3	-9.46 ± 0.83	1.03 ± 0.11	1099 ± 554	5.27 ± 1.10	FeII
2016-10a	Silver	3.80 ± 0.60	35.5 ± 13.0	-7.39 ± 1.12	1.21 ± 0.10	538 ± 501	1.71 ± 1.20	...

Table 5. Recurrent Nova Parameters

RN (M31N)	Quality	L_4 ($10^4 L_\odot$)	t_2 (days)	$\log \dot{M}$ ($M_\odot \text{ yr}^{-1}$)	M_{WD} (M_\odot)	V_{max} (km s^{-1})	P_{rec} (yr)	$P_{\text{rec(obs)}}$ (yr)	Type	Notes ^a
1923-12c	Silver	4.17 ± 0.79	12.6 ± 0.9	-7.01 ± 0.91	1.32 ± 0.07	641 ± 490	3.2	9.5	He/N	1
1926-07c	Gold	4.37 ± 1.01	11.1 ± 1.4	$-7.00 :$	1.33 ± 0.07	667 ± 556	2.7	2.7	He/Nn	2
1960-12a	Bronze	3.47 ± 0.55	4.7 ± 0.2	$-7.00 :$	1.39 ± 0.02	920 ± 398	1.1	6.2	He/N	3
1963-09c	Bronze	3.02 ± 0.48	4.0 ± 0.5	$-7.00 :$	1.37 ± 0.00	826 ± 335	1.5	5.0	He/N	4
1966-09e	Silver	1.82 ± 0.34	13.0 ± 1.5	-7.01 ± 0.41	1.31 ± 0.05	586 ± 295	4.2	40.9	FeII:	5
1984-07a	Silver	15.00 ± 3.33	9.7 ± 1.5	-10.34 ± 0.26	1.24 ± 0.02	2877 ± 749	3.16E5	9.4	FeIIB	6
1990-10a	Silver	4.33 ± 0.68	11.1 ± 1.7	$-7.00 :$	1.33 ± 0.06	670 ± 504	2.7	5.3	FeIIB	7
1997-11k	Silver	1.66 ± 0.26	110 ± 29	-7.01 ± 0.84	1.12 ± 0.15	283 ± 229	39.9	4.0	FeII:	8
2006-11c	Bronze	11.07 ± 1.51	1.8 ± 0.5	-9.00 ± 0.39	1.38 ± 0.01	3750 ± 1357	814.7	8.2	He/N	9
2007-10b	Bronze	2.09 ± 0.43	2.7 ± 0.6	$-7.00 :$	1.39 ± 0.03	899 ± 397	1.2	10.2	He/N	10
2007-11f	Bronze	5.30 ± 0.80	10.2 ± 2.6	-7.83 ± 0.68	1.28 ± 0.04	1042 ± 628	86.9	9.1	He/Nn	11
2008-12a	Gold	2.17 ± 0.21	2.2 ± 0.1	-7.08 ± 0.04	1.40 ± 0.01	1047 ± 438	1.2	1.0	He/N	12
2013-10c	Gold	19.95 ± 3.16	5.5 ± 1.7	-10.44 ± 0.23	1.31 ± 0.02	4130 ± 1160	1.75E5	10.1	...	13
2017-01e	...	3.47 ± 0.71	5.2 ± 1.6	$-7.00 :$	1.38 ± 0.02	885 ± 383	1.2	2.5	He/N	14

^a With the exception of M31N 2017-01e, outburst data are from Clark et al. (2024) and are based on the following outbursts: (1) 2012-01b; (2) 2020-01b, 2022-09a; (3) 2013-05b; (4) 2010-10e, 2015-10c; (5) 2007-08d; (6) 2012-09a, 2022-11b; (7) 2016-07e; (8) 2009-11b; (9) 2015-02b; (10) 2007-10b, 2017-12a; (11) 2007-11f, 2016-12e; (12) 2008-12a, and subsequent outbursts from Burris et al. (2023); (13) 2013-10c; (14) 2024-08c (Shafter et al. 2024a).

Table 6. M31 Nova Parameters

Parameter	Linear	Break	Jitter	Fe II	He/N ^a	RNe	All M31
$\langle M_{WD} \rangle (M_{\odot})$	1.15 ± 0.11	1.18 ± 0.12	1.00 ± 0.15	1.12 ± 0.14	1.26 ± 0.12	1.33 ± 0.08	1.15 ± 0.14
$\langle M_{WD} \rangle (\text{Gold}) (M_{\odot})$	1.16 ± 0.09	1.20 ± 0.10	1.35 ± 0.05	1.19 ± 0.10
$\langle M_{WD} \rangle (\text{Silver}) (M_{\odot})$	1.13 ± 0.08	1.14 ± 0.13	1.10 ± 0.15	1.26 ± 0.09	1.14 ± 0.11
$\langle M_{WD} \rangle (\text{Bronze}) (M_{\odot})$	1.16 ± 0.15	1.12 ± 0.16	0.99 ± 0.15	1.36 ± 0.05	1.11 ± 0.18
$\langle \log \dot{M} \rangle (M_{\odot} \text{ yr}^{-1})$	-9.27 ± 1.39	-10.04 ± 1.09	-8.59 ± 1.08	-9.34 ± 1.40	-8.77 ± 1.65	-7.69 ± 1.27	-9.27 ± 1.41
$\langle V_{\max} \rangle (\text{km s}^{-1})$	1568 ± 1215	2457 ± 1560	757 ± 306	1610 ± 1390	1903 ± 1501	1373 ± 1241	1690 ± 1361
$\langle \log P_{\text{rec}} \rangle (\text{yr})$	4.44 ± 2.01	5.28 ± 1.49	4.04 ± 1.79	4.61 ± 1.94	3.17 ± 2.54	1.40 ± 1.88	4.39 ± 2.06

^a Including Fe IIb (Hybrid) novae

Table 7. Variation of Nova Parameters with Isophotal Radius^a

Parameter	Mean (bulge)	σ_{mean} (bulge)	Mean (disk)	σ_{mean} (disk)	Significance
$\log L_4$	0.897 ± 0.346	0.0300	0.739 ± 0.343	0.0523	2.6σ
$\log t_2$	1.375 ± 0.388	0.0338	1.355 ± 0.435	0.0663	0.27σ
M_{WD}	1.145 ± 0.134	0.0117	1.167 ± 0.159	0.0243	0.82σ
$\log \dot{M}$	-9.451 ± 1.358	0.118	-8.719 ± 1.444	0.220	2.9σ
$\log V_{\max}$	3.141 ± 0.314	0.0273	3.025 ± 0.320	0.0487	2.1σ
$\log P_{\text{rec}}$	4.659 ± 1.945	0.169	3.557 ± 2.210	0.337	2.9σ

^a We define the bulge to include isophotal radii $a \leq 15'$ and the disk for $a > 15'$.

REFERENCES

- Arp, H. C. 1956, AJ, 61, 15, doi: [10.1086/107284](https://doi.org/10.1086/107284)
- Aydi, E., Chomiuk, L., Strader, J., et al. 2024, MNRAS, 527, 9303, doi: [10.1093/mnras/stad3342](https://doi.org/10.1093/mnras/stad3342)
- Bland-Hawthorn, J., & Gerhard, O. 2016, ARA&A, 54, 529, doi: [10.1146/annurev-astro-081915-023441](https://doi.org/10.1146/annurev-astro-081915-023441)
- Burris, W. A., Shafter, A. W., & Hornoch, K. 2023, Research Notes of the American Astronomical Society, 7, 179, doi: [10.3847/2515-5172/acf220](https://doi.org/10.3847/2515-5172/acf220)
- Ciardullo, R., Ford, H. C., Neill, J. D., Jacoby, G. H., & Shafter, A. W. 1987, ApJ, 318, 520, doi: [10.1086/165388](https://doi.org/10.1086/165388)
- Clark, J. G., Hornoch, K., Shafter, A. W., et al. 2024, ApJS, 272, 28, doi: [10.3847/1538-4365/ad3c39](https://doi.org/10.3847/1538-4365/ad3c39)
- Cohen, A., Guetta, D., Hillman, Y., et al. 2025, ApJ, 981, 198, doi: [10.3847/1538-4357/adb628](https://doi.org/10.3847/1538-4357/adb628)
- Craig, P., Aydi, E., Chomiuk, L., et al. 2025, MNRAS, 538, 2339, doi: [10.1093/mnras/staf385](https://doi.org/10.1093/mnras/staf385)
- Curtin, C., Shafter, A. W., Pritchett, C. J., et al. 2015, ApJ, 811, 34, doi: [10.1088/0004-637X/811/1/34](https://doi.org/10.1088/0004-637X/811/1/34)
- Darnley, M. J., Williams, S. C., Bode, M. F., et al. 2014, A&A, 563, L9, doi: [10.1051/0004-6361/201423411](https://doi.org/10.1051/0004-6361/201423411)
- Darnley, M. J., Bode, M. F., Kerins, E., et al. 2004, MNRAS, 353, 571, doi: [10.1111/j.1365-2966.2004.08087.x](https://doi.org/10.1111/j.1365-2966.2004.08087.x)
- . 2006, MNRAS, 369, 257, doi: [10.1111/j.1365-2966.2006.10297.x](https://doi.org/10.1111/j.1365-2966.2006.10297.x)
- Darnley, M. J., Henze, M., Bode, M. F., et al. 2016, ApJ, 833, 149, doi: [10.3847/1538-4357/833/2/149](https://doi.org/10.3847/1538-4357/833/2/149)
- De, K., Kasliwal, M. M., Hankins, M. J., et al. 2021, ApJ, 912, 19, doi: [10.3847/1538-4357/abeb75](https://doi.org/10.3847/1538-4357/abeb75)
- de Vaucouleurs, G., de Vaucouleurs, A., Corwin, Herold G., J., et al. 1991, Third Reference Catalogue of Bright Galaxies
- Della Valle, M., & Izzo, L. 2020a, A&A Rv, 28, 3, doi: [10.1007/s00159-020-0124-6](https://doi.org/10.1007/s00159-020-0124-6)
- . 2020b, A&A Rv, 28, 3, doi: [10.1007/s00159-020-0124-6](https://doi.org/10.1007/s00159-020-0124-6)
- Della Valle, M., & Livio, M. 1998, ApJ, 506, 818, doi: [10.1086/306275](https://doi.org/10.1086/306275)
- Della Valle, M., Rosino, L., Bianchini, A., & Livio, M. 1994, A&A, 287, 403
- Ford, G. P., Gear, W. K., Smith, M. W. L., et al. 2013, ApJ, 769, 55, doi: [10.1088/0004-637X/769/1/55](https://doi.org/10.1088/0004-637X/769/1/55)
- Ford, H. C. 1978, ApJ, 219, 595, doi: [10.1086/155819](https://doi.org/10.1086/155819)
- Hillman, Y., Shara, M. M., Prialnik, D., & Kovetz, A. 2020, Nature Astronomy, 4, 886, doi: [10.1038/s41550-020-1062-y](https://doi.org/10.1038/s41550-020-1062-y)

- Hornoč, K., Kučáková, H., & Shafter, A. W. 2022, The Astronomer's Telegram, 15545, 1
- Hornoč, K., & Shafter, A. W. 2015, The Astronomer's Telegram, 7116, 1
- Hubble, E. P. 1929, ApJ, 69, 103, doi: [10.1086/143167](https://doi.org/10.1086/143167)
- Kato, M., Saio, H., Hachisu, I., & Nomoto, K. 2014, ApJ, 793, 136, doi: [10.1088/0004-637X/793/2/136](https://doi.org/10.1088/0004-637X/793/2/136)
- Kawash, A., Chomiuk, L., Strader, J., et al. 2022, ApJ, 937, 64, doi: [10.3847/1538-4357/ac8d5e](https://doi.org/10.3847/1538-4357/ac8d5e)
- Knigge, C. 2011, in Astronomical Society of the Pacific Conference Series, Vol. 447, Evolution of Compact Binaries, ed. L. Schmidtobreick, M. R. Schreiber, & C. Tappert, 3, doi: [10.48550/arXiv.1108.4716](https://doi.org/10.48550/arXiv.1108.4716)
- Kurtenkov, A. A., Peshev, P., Tomov, T., et al. 2015, A&A, 578, L10, doi: [10.1051/0004-6361/201526564](https://doi.org/10.1051/0004-6361/201526564)
- Licquia, T. C., & Newman, J. A. 2015, ApJ, 806, 96, doi: [10.1088/0004-637X/806/1/96](https://doi.org/10.1088/0004-637X/806/1/96)
- Mandel, S., Shara, M. M., Zurek, D., Conroy, C., & van Dokkum, P. 2023, MNRAS, 518, 5279, doi: [10.1093/mnras/stac2960](https://doi.org/10.1093/mnras/stac2960)
- McConnachie, A. W., Irwin, M. J., Ferguson, A. M. N., et al. 2005, MNRAS, 356, 979, doi: [10.1111/j.1365-2966.2004.08514.x](https://doi.org/10.1111/j.1365-2966.2004.08514.x)
- Nomoto, K., Saio, H., Kato, M., & Hachisu, I. 2007, ApJ, 663, 1269
- Pecaut, M. J., & Mamajek, E. E. 2013, ApJS, 208, 9, doi: [10.1088/0067-0049/208/1/9](https://doi.org/10.1088/0067-0049/208/1/9)
- Pritchett, C. J., & van den Bergh, S. 1987, ApJ, 318, 507, doi: [10.1086/165387](https://doi.org/10.1086/165387)
- Rappaport, S., Verbunt, F., & Joss, P. C. 1983, ApJ, 275, 713, doi: [10.1086/161569](https://doi.org/10.1086/161569)
- Rector, T. A., Shafter, A. W., Burris, W. A., et al. 2022, ApJ, 936, 117, doi: [10.3847/1538-4357/ac87ad](https://doi.org/10.3847/1538-4357/ac87ad)
- Ritchey, G. W. 1917, PASP, 29, 210, doi: [10.1086/122638](https://doi.org/10.1086/122638)
- Rosino, L. 1964, Annales d'Astrophysique, 27, 498
- . 1973, A&AS, 9, 347
- Schaefer, B. E. 2018, MNRAS, 481, 3033, doi: [10.1093/mnras/sty2388](https://doi.org/10.1093/mnras/sty2388)
- . 2022, MNRAS, 517, 6150, doi: [10.1093/mnras/stac2900](https://doi.org/10.1093/mnras/stac2900)
- . 2025, ApJ, 993, 232, doi: [10.3847/1538-4357/ae0616](https://doi.org/10.3847/1538-4357/ae0616)
- Selvelli, P., & Gilmozzi, R. 2019, A&A, 622, A186, doi: [10.1051/0004-6361/201834238](https://doi.org/10.1051/0004-6361/201834238)
- Shafter, A. W. 2017, ApJ, 834, 196, doi: [10.3847/1538-4357/834/2/196](https://doi.org/10.3847/1538-4357/834/2/196)
- . 2019, Extragalactic Novae; A historical perspective, doi: [10.1088/2514-3433/ab2c63](https://doi.org/10.1088/2514-3433/ab2c63)
- Shafter, A. W., & Hornoch, K. 2025, The Astronomer's Telegram, 17182, 1
- Shafter, A. W., Hornoch, K., Ciardullo, J. V. R., Darnley, M. J., & Bode, M. F. 2012, The Astronomer's Telegram, 4503, 1
- Shafter, A. W., & Irby, B. K. 2001, ApJ, 563, 749, doi: [10.1086/324044](https://doi.org/10.1086/324044)
- Shafter, A. W., Kundu, A., & Henze, M. 2017, Research Notes of the American Astronomical Society, 1, 11, doi: [10.3847/2515-5172/aa9847](https://doi.org/10.3847/2515-5172/aa9847)
- Shafter, A. W., Taguchi, K., Zhao, J., & Hornoch, K. 2022a, Research Notes of the American Astronomical Society, 6, 241, doi: [10.3847/2515-5172/aca2a6](https://doi.org/10.3847/2515-5172/aca2a6)
- Shafter, A. W., Darnley, M. J., Hornoch, K., et al. 2011, ApJ, 734, 12, doi: [10.1088/0004-637X/734/1/12](https://doi.org/10.1088/0004-637X/734/1/12)
- Shafter, A. W., Henze, M., Rector, T. A., et al. 2015, ApJS, 216, 34, doi: [10.1088/0067-0049/216/2/34](https://doi.org/10.1088/0067-0049/216/2/34)
- Shafter, A. W., Hornoch, K., Kučáková, H., et al. 2022b, Research Notes of the American Astronomical Society, 6, 214, doi: [10.3847/2515-5172/ac9ab9](https://doi.org/10.3847/2515-5172/ac9ab9)
- Shafter, A. W., Hornoch, K., Zhao, J., et al. 2022c, The Astronomer's Telegram, 15729, 1
- Shafter, A. W., Zhao, J., Hornoch, K., et al. 2024a, Research Notes of the American Astronomical Society, 8, 256, doi: [10.3847/2515-5172/ad84d5](https://doi.org/10.3847/2515-5172/ad84d5)
- Shafter, A. W., Hornoch, K., Kučáková, H., et al. 2024b, Research Notes of the American Astronomical Society, 8, 5, doi: [10.3847/2515-5172/ad19de](https://doi.org/10.3847/2515-5172/ad19de)
- Shara, M. M. 1981, ApJ, 243, 926, doi: [10.1086/158657](https://doi.org/10.1086/158657)
- . 1989, PASP, 101, 5, doi: [10.1086/132400](https://doi.org/10.1086/132400)
- Shara, M. M., Livio, M., Moffat, A. F. J., & Orio, M. 1986, ApJ, 311, 163, doi: [10.1086/164762](https://doi.org/10.1086/164762)
- Shara, M. M., Prihnik, D., Hillman, Y., & Kovetz, A. 2018, ApJ, 860, 110, doi: [10.3847/1538-4357/aabfb](https://doi.org/10.3847/1538-4357/aabfb)
- Shara, M. M., Doyle, T. F., Lauer, T. R., et al. 2016, ApJS, 227, 1, doi: [10.3847/0067-0049/227/1/1](https://doi.org/10.3847/0067-0049/227/1/1)
- Shara, M. M., Lessing, A. M., Hounsell, R., et al. 2023, ApJS, 269, 42, doi: [10.3847/1538-4365/ad02fd](https://doi.org/10.3847/1538-4365/ad02fd)
- Sick, J., Courteau, S., Cuillandre, J.-C., et al. 2015, in IAU Symposium, Vol. 311, Galaxy Masses as Constraints of Formation Models, ed. M. Cappellari & S. Courteau, 82–85, doi: [10.1017/S1743921315003440](https://doi.org/10.1017/S1743921315003440)
- Sin, P., Henze, M., Sala, G., et al. 2017, The Astronomer's Telegram, 10001, 1
- Socia, Q., Henze, M., Shafter, A. W., & Horst, J. C. 2018, Research Notes of the American Astronomical Society, 2, 190, doi: [10.3847/2515-5172/aae7ce](https://doi.org/10.3847/2515-5172/aae7ce)
- Starrfield, S., Iliadis, C., & Hix, W. R. 2016, PASP, 128, 051001, doi: [10.1088/1538-3873/128/963/051001](https://doi.org/10.1088/1538-3873/128/963/051001)
- Tang, S., Bildsten, L., Wolf, W. M., et al. 2014, ApJ, 786, 61, doi: [10.1088/0004-637X/786/1/61](https://doi.org/10.1088/0004-637X/786/1/61)

- Torres, G. 2010, AJ, 140, 1158,
doi: [10.1088/0004-6256/140/5/1158](https://doi.org/10.1088/0004-6256/140/5/1158)
- Townsley, D. M., & Bildsten, L. 2004, ApJ, 600, 390,
doi: [10.1086/379701](https://doi.org/10.1086/379701)
- . 2005, ApJ, 628, 395, doi: [10.1086/430594](https://doi.org/10.1086/430594)
- Warner, B. 2003, Cataclysmic Variable Stars,
doi: [10.1017/CBO9780511586491](https://doi.org/10.1017/CBO9780511586491)
- Williams, B. F., Dalcanton, J. J., Dolphin, A. E., et al.
2015, ApJ, 806, 48, doi: [10.1088/0004-637X/806/1/48](https://doi.org/10.1088/0004-637X/806/1/48)
- Williams, R. E. 1992, AJ, 104, 725, doi: [10.1086/116268](https://doi.org/10.1086/116268)
- Williams, S. J., & Shafter, A. W. 2004, ApJ, 612, 867,
doi: [10.1086/422833](https://doi.org/10.1086/422833)
- Wolf, W. M., Bildsten, L., Brooks, J., & Paxton, B. 2013,
ApJ, 777, 136, doi: [10.1088/0004-637X/777/2/136](https://doi.org/10.1088/0004-637X/777/2/136)
- Yaron, O., Prialnik, D., Shara, M. M., & Kovetz, A. 2005,
The Astrophysical Journal, 623, 398, doi: [10.1086/428436](https://doi.org/10.1086/428436)
- Yungelson, L., Livio, M., & Tutukov, A. 1997, ApJ, 481,
127, doi: [10.1086/304020](https://doi.org/10.1086/304020)
- Zorotovic, M., & Schreiber, M. R. 2020, Advances in Space
Research, 66, 1080, doi: [10.1016/j.asr.2019.08.044](https://doi.org/10.1016/j.asr.2019.08.044)

Table A1. M31 Recurrent Novae

Recurrent Nova	R.A. (h,m,s)	Decl. ($^{\circ}, ', ''$)	N_{rec}	$\langle \Delta t \rangle$ (yr)	$\langle M_R \rangle$ (max)	$\langle t_2 \rangle$ (d)	$a (')$	Type	References ^a
M31N1919-09a	0 43 28.65	41 21 42.1	1	78.7	10.50	...	1
M31N1923-12c	0 42 38.07	41 08 41.4	2	9.5	-6.96 ± 0.18	12.6 ± 0.9	10.99	He/N	1,2
M31N1926-06a	0 41 40.66	41 03 33.7	1	36.5	...	$\gtrsim 5$	17.43	...	1
M31N1926-07c	0 42 52.37	41 16 12.8	4	2.7	-7.01 ± 0.20	11.1 ± 1.4	1.68	He/Nn	1,2,3
M31N1945-09c	0 41 28.58	40 53 13.7	1	27.0	29.19	...	1
M31N1953-09b:	0 42 20.69	41 16 07.9	1	50.8	5.77	...	1
M31N1960-12a	0 42 55.71	41 14 12.5	2	6.2	-6.76 ± 0.14	4.7 ± 0.2	4.40	He/N	1,2
M31N1961-11a:	0 42 31.36	41 16 21.0	1	43.6	3.03	...	1
M31N1963-09c	0 42 57.75	41 08 12.3	6	5.0	-6.61 ± 0.14	4.0 ± 0.5	17.60	He/N	1,2
M31N1966-09e	0 39 30.33	40 29 14.0	1	40.9	-6.06 ± 0.18	13.0 ± 1.5	59.56	Fe II	1,2
M31N1982-08b	0 46 06.68	42 03 49.3	1	14.9	60.83	...	1
M31N1984-07a	0 42 47.15	41 16 19.6	3	9.4	-8.35 ± 0.11	9.7 ± 1.5	0.57	Fe IIb	1,2
M31N1990-10a	0 43 04.00	41 17 08.1	3	5.3	-7.00 ± 0.14	11.1 ± 1.7	4.28	Fe IIb	1,2
M31N1997-11k	0 42 39.60	41 09 02.9	3	4.0	-5.96 ± 0.14	110 ± 29	10.57	Fe II	1,2
M31N2001-11a	0 44 14.55	41 22 04.2	1	23.2	~ -7.5	~ 8	27.90	...	4
M31N2005-10a	0 44 20.70	41 23 11.0	1	16.8	29.43	...	5
M31N2006-11c	0 41 33.17	41 10 12.4	1	8.2	-8.02 ± 0.11	1.8 ± 0.5	19.82	He/N	2,6
M31N2007-10b	0 43 29.47	41 17 13.9	1	10.2	-6.21 ± 0.20	2.7 ± 0.6	12.90	He/N	2,7
M31N2007-11f	0 41 31.54	41 07 13.6	1	9.1	-7.22 ± 0.13	10.2 ± 2.6	18.90	He/Nn	2,8
M31N2008-12a	0 45 28.80	41 54 10.1	21	1.0	-6.25 ± 0.04	2.2 ± 0.1	48.92	He/N	1,2,9,10,11
M31N2013-10c	0 43 09.54	41 15 39.9	1	10.1	-8.66 ± 0.14	5.5 ± 1.7	6.38	...	2,12
M31N2017-01e	0 44 10.72	41 54 22.1	5	2.5	-6.76 ± 0.20	5.2 ± 1.6	54.19	He/N	13,14,15

^a (1) Shafter et al. (2015); (2) Clark et al. (2024); (3) Shafter et al. (2022b); (4) Shafter & Hornoch (2025); (5) Hornoch et al. (2022); (6) Hornoch & Shafter (2015); (7) Socia et al. (2018); (8) Sin et al. (2017); (9) Shafter et al. (2012); (10) Darnley et al. (2016); (11) Burris et al. (2023); (12) Shafter et al. (2024b); (13) Shafter et al. (2022c); (14) Shafter et al. (2022a); (15) Shafter et al. (2024a)

APPENDIX

For completeness, in this appendix we summarize in Table A1 the observed properties, including equatorial coordinates (J2000), of the 22 known or suspected M31 RNe as of 2026 January 1. Two of these systems, M31N 1953-09b and 1961-11a, will require confirmation before their recurrent nature can be firmly established. Photometric data sufficient to establish the peak absolute magnitude, $M_R(\text{max})$, and t_2 time are available for just 14 of the 22 systems. These are the 14 RNe that have been analyzed in this paper (see Table 5).